Cellular/Molecular

Peptide Inhibitors Disrupt the Serotonin 5-HT$_{2C}$ Receptor Interaction with Phosphatase and Tensin Homolog to Allosterically Modulate Cellular Signaling and Behavior

Noelle C. Anastasio,[1,2] Scott R. Gilbertson,[1,4] Marcy J. Bubar,[1] Anton Agarkov,[4] Sonja J. Stutz,[1,2] Yowjiun Jeng,[1,2,3] Nicole M. Bremer,[1,2] Thressa D. Smith,[1,2] Robert G. Fox,[1,2] Sarah E. Swinford,[1] Patricia K. Seitz,[1,2] Marc N. Charendoff,[5] John W. Craft Jr,[5] Fernanda M. Laezza,[1,2] Cheryl S. Watson,[1,3] James M. Briggs,[5] and Kathryn A. Cunningham[1,2]

[1]Center for Addiction Research and Departments of [2]Pharmacology and Toxicology and [3]Biochemistry and Molecular Biology, University of Texas Medical Branch, Galveston, Texas 77555, and Departments of [4]Chemistry and [5]Biology and Biochemistry, University of Houston, Houston, Texas 77004

Serotonin (5-hydroxytryptamine; 5-HT) signaling through the 5-HT$_{2C}$ receptor (5-HT$_{2C}$R) is essential in normal physiology, whereas aberrant 5-HT$_{2C}$R function is thought to contribute to the pathogenesis of multiple neural disorders. The 5-HT$_{2C}$R interacts with specific protein partners, but the impact of such interactions on 5-HT$_{2C}$R function is poorly understood. Here, we report convergent cellular and behavioral data that the interaction between the 5-HT$_{2C}$R and protein phosphatase and tensin homolog (PTEN) serves as a regulatory mechanism to control 5-HT$_{2C}$R-mediated biology but not that of the closely homologous 5-HT$_{2A}$R. A peptide derived from the third intracellular loop of the human 5-HT$_{2C}$R [3L4F (third loop, fourth fragment)] disrupted the association, allosterically augmented 5-HT$_{2C}$R-mediated signaling in live cells, and acted as a positive allosteric modulator in rats *in vivo*. We identified the critical residues within an 8 aa fragment of the 3L4F peptide that maintained efficacy (within the picomolar range) in live cells similar to that of the 3L4F peptide. Last, molecular modeling identified key structural features and potential interaction sites of the active 3L4F peptides against PTEN. These compelling data demonstrate the specificity and importance of this protein assembly in cellular events and behaviors mediated by 5-HT$_{2C}$R signaling and provide a chemical guidepost to the future development of drug-like peptide or small-molecule inhibitors as neuroprobes to study 5-HT$_{2C}$R allostery and therapeutics for 5-HT$_{2C}$R-mediated disorders.

Introduction

Serotonin (5-HT) signaling through the 5-HT$_{2C}$ receptor (5-HT$_{2C}$R) is essential in normal physiology (e.g., appetite) (Heisler et al., 2003) and influences the pathogenesis of psychiatric (e.g., addictions), neurological (e.g., epilepsy), and eating and metabolic disorders (Bubar and Cunningham, 2008; Kennett and Clifton, 2010; Rosenzweig-Lipson, 2011). This G-protein-coupled receptor (GPCR) is expressed prominently in brain (Mengod et al., 1990), particularly within limbic–corticostriatal circuitry involved in reward, motivation, and cognition (Pompeiano et al., 1994; Mengod et al., 1996; Liu et al., 2007; Anastasio et al., 2010). The 5-HT$_{2C}$R undergoes a dynamic conformational change during agonist binding and activation of intracellular signaling. Best characterized is coupling of the 5-HT$_{2C}$R to G$\alpha_{q/11}$ to activate phospholipase-Cβ-mediated signaling, leading to increased intracellular calcium release and activation of downstream effectors (Raymond et al., 2001; Millan et al., 2008).

The sequence of ligand binding to a GPCR and subsequent activation of downstream signaling can be positively or negatively modulated by binding of ligands at allosteric sites topographically distinct from the orthosteric ligand binding site (Agnati et al., 2011; Melancon et al., 2012). There are theoretical reasons (i.e., increased selectivity, upper ceiling effects, separate control of affinity and efficacy) as to why allosteric ligands may be preferred therapeutic chemical targets (Kenakin, 2010). Therefore, 5-HT$_{2C}$R allosteric modulators present a novel drug design strategy (Im et al., 2003; Ding et al., 2012) to selectively tune up or down signaling in response to endogenous 5-HT in a site- and event-specific manner (Conn et al., 2009). Allostery could also be promoted through protein–protein interactions at the 5-HT$_{2C}$R cytosolic face (Bécamel et al., 2002; Labasque et al., 2008), but the functional impact of such interactions over 5-HT$_{2C}$R signaling is little studied. A protein–protein interaction of interest is the association between the third intracellular loop of the 5-HT$_{2C}$R and protein phosphatase and tensin homolog (PTEN). A peptide

Received June 2, 2012; revised Oct. 10, 2012; accepted Nov. 16, 2012.

Author contributions: N.C.A., S.R.G., M.J.B., C.S.W., J.M.B., and K.A.C. designed research; N.C.A., S.R.G., A.A., S.J.S., Y.J., N.M.B., T.D.S., R.G.F., S.E.S., P.K.S., M.N.C., J.W.C., and K.A.C. performed research; N.C.A., S.R.G., A.A., S.J.S., Y.J., N.M.B., T.D.S., R.G.F., S.E.S., P.K.S., M.N.C., J.W.C., F.M.L., C.S.W., J.M.B., and K.A.C. analyzed data; N.C.A., S.R.G., M.J.B., M.N.C., J.W.C., J.M.B., and K.A.C. wrote the paper.

This work was supported by the Klarman Family Foundation, the Foundation for Prader-Willi Research, and National Institute of Drug Abuse Grants DA06511, DA024157, and DA020087. K.A.C. is an editor of *Neuropsychopharmacology Reviews* and receives compensation for this role from the American College of Neuropsychopharmacology. We thank Drs. Kelly Berg and William Clarke from the University of Texas Health Science Center at San Antonio for the gift of the CHO cell lines. We thank Dr. Adriana Paulucci-Holthauzen and Leoncio Vergara with the University of Texas Medical Branch Optical Microscopy Core for capturing confocal microscopy images and contributing to analysis of confocal photomicrographs. The NAMD (Not Another Molecular Dynamics) program was developed by the Theoretical and Computational Biophysics Group in the Beckman Institute for Advanced Science and Technology at the University of Illinois at Urbana-Champaign.

Correspondence should be addressed to Dr. Kathryn A. Cunningham, University of Texas Medical Branch Center for Addiction Research, University of Texas Medical Branch, Galveston, TX 77555-0615. E-mail: kcunning@utmb.edu.

DOI:10.1523/JNEUROSCI.2656-12.2013

 0270-6474/13/331615-16$15.00/0

fragment of the 5-HT_{2C}R third intracellular loop [3L4F (third loop, fourth fragment)] was reported to disrupt the 5-HT_{2C}R–PTEN complex as well as PTEN-mediated dephosphorylation of 5-HT_{2C}R in PC12 cells (Ji et al., 2006). The 3L4F peptide, conjugated to the cell-penetrant TAT, exhibited an initial *in vivo* profile consistent with 5-HT_{2C}R agonism in rats (Ji et al., 2006). Given the role of the 5-HT_{2C}R third intracellular loop in G-protein selectivity and activation (Cheung et al., 1992), the 5-HT_{2C}R–PTEN complex may regulate 5-HT_{2C}R coupling to its effector pathway(s), and disruption of the 5-HT_{2C}R–PTEN complex may enhance 5-HT_{2C}R-mediated signaling.

Here, we further investigated the function of the 5-HT_{2C}R–PTEN complex. We show that this protein–protein interaction mediates a saturable and positive allosterism of 5-HT_{2C}R over downstream signaling in live cells and is specific to 5-HT_{2C}R relative to the homologous 5-HT_{2A}R. We provide evidence that 3L4F is a positive allosteric modulator in rats *in vivo*. Last, molecular modeling identified key structural features and potential interaction sites of the active 3L4F peptide derivatives. Convergent cellular, behavioral, and modeling data demonstrate a distinct role for the 5-HT_{2C}R–PTEN complex in 5-HT_{2C}R signaling, define positive allosteric modulatory actions of new peptide disrupters, and provide models that predict the pharmacophore for the active peptides.

Materials and Methods

Cell lines and cell culture

The parental Chinese hamster ovary (CHO) K1, the 5-HT_{2A}R–CHO, and 5-HT_{2C}R–CHO cell lines were generous gifts from Drs. K. Berg and W. Clarke from the University of Texas Health Science Center at San Antonio (San Antonio, TX). The 5-HT_{2A}R line was transfected with the human 5-HT_{2A}R, and the 5-HT_{2C}R line was transfected with the nonedited human 5-HT_{2C}R in the p198–DHFR–Hygro vector containing a hygromycin resistance gene (Berg et al., 1994). Reverse transcription of RNA followed by quantitative real-time PCR confirmed (data not shown) that the 5-HT_{2A}R–CHO cell line expressed the human 5-HT_{2A}R transcript but not the human 5-HT_{2C}R transcript or protein (Berg et al., 2001). The 5-HT_{2C}R–CHO cell line expressed the human 5-HT_{2C}R transcript but not the human 5-HT_{2A}R transcript (Berg et al., 2001), and the parental cell line did not express detectable amounts of either mRNA or protein (Berg et al., 2001; Anastasio et al., 2010). Cells were grown in GlutaMax–αMEM (Invitrogen) at 37°C, 5% CO_2, and 85% relative humidity and were passaged at 80% confluence.

Ligands

5-HT (Acros Organics, Thermo Fisher Scientific) was dissolved in 1× HBSS (Cellgro; Invitrogen). WAY163909 [(7b*R*, 10a*R*)-1,2,3,4,8,9,10,10a-octahydro-7b*H*-cyclopenta-(b)(1,4)diazepino (6,7,1hi)indole; a gift from Pfizer] was dissolved in 0.9% NaCl. SB242084 [6-chloro-5-methyl-1-((2-(2-methylpyrid-3-yloxy) pyrid-5-yl)carbamoyl)indoline dihydrochloride; Sigma] was dissolved in 1× HBSS containing 10 mmol/L citric acid (Sigma) and 8% 2-hydroxypropyl-β-cyclodextrin (Trappsol Hydroxypropyl Beta Cyclodextrin, pharmaceutical grade; Cyclodextrin Technologies Development) with the final pH adjusted to 5.6.

Peptides

The 3L4F peptide (Ac-PNQDQNARRRKKKERR-NH_2; Pro280–Arg295 of the human 5-HT_{2C}R) and the 3L4F peptide fragments [3L4F-F_1 (Ac-PNQDQNAR-NH_2; Pro280–Arg287 of the human 5-HT_{2C}R), 3L4F-F_2 (Ac-QNARRRKK-NH_2; Gln284–Lys291 of the human 5-HT_{2C}R), and 3L4F-F_3 (Ac-RRKKKERR-NH_2; Arg288–Arg295 of the human 5-HT_{2C}R)] were synthesized by Drs. Anton Agarkov and Scott R. Gilbertson (University of Houston, Houston, TX) and dissolved in HBSS for cellular studies. The 3L4F and 3L4F fragment peptides were first synthesized on solid supports using standard FMOC chemistry, cleaved from the solid support, and purified (>95%) by HPLC, and characterized by mass spectrometry. The rat TAT–3L4F peptide [Ac-YGRKKRRQRRRPNPDQKPRRKKKEKR-NH_2; TAT–Pro283–Arg297 of the rat 5-HT_{2C}R (Ji et al., 2006)] was synthesized and HPLC purified by GenScript and dissolved in HBSS for cellular studies and 0.9% NaCl for behavioral studies.

Peptide modeling and docking

Replica exchange molecular dynamics (REMD) (Sugita and Okamoto, 1999) simulations were performed on both the 3L4F and 3L4F-F_1 peptides using the temperature intervals with global energy reassignment strategy (Li et al., 2009) to predict the secondary structural content of the peptides. Molecular dynamics simulations for all simulation runs were performed using the parallel molecular dynamics software NAMD 2.6 [Not Another Molecular Dynamics Program (Phillips et al., 2005)] to compute dynamics trajectories using the CHARMM 27 (Chemistry at Harvard Macromolecular Mechanics 27) empirical force field (MacKerell et al., 1998). The 3L4F and 3L4F-F_1 peptides were first generated in the extended conformation, followed by solvation with TIP3 explicit water molecules (Price and Brooks, 2004), after which counter ions were inserted to neutralize the system. Molecular dynamics trajectories were run for 50 ns each at 300,000, 378,000, 476,000, and 600,000 with an exchange frequency of 3 ps. The resultant 300,000 molecular dynamics trajectories were examined for secondary structure using dihedral principal component analysis [dPCA; implemented in *Carma* (Glykos, 2006)] because these conditions are the most physiologically relevant. The 3L4F-F_1 peptide conformations were subject to coarse-grained cluster docking against the crystal structure of PTEN (Research Collaboratory for Structural Bioinformatics Protein Data Bank; www.rcsb.org; identification number 1D5R) using GRAMM [Global Range Molecular Matching (Vakser and Aflalo, 1994)] to predict the structural interaction of 3L4F-F_1 with PTEN.

Circular dichroism (CD) analysis of protein conformations was used to experimentally evaluate the secondary structural content of the 3L4F and 3L4F-F_1 peptides for comparison with the computational molecular dynamics simulation predictions (above). The spectra were collected on an OLIS 1000 spectrophotometer with scans from 195 to 255 nm averaged over three trial scans and 140 points with 2400 grating lines/mm. The instrument was calibrated with 250 μg/ml camphor sulfonic acid and 300 μg/ml BSA, and 3L4F and 3L4F-F_1 samples were prepared in 100 or 300 μM concentrations in water to adjust the signal/noise resolution. The data were compared with Fasman standards (Greenfield and Fasman, 1969) supplemented with data for β-turns (Holde et al., 1998).

Physical analyses of 5-HT_{2C}R–PTEN interaction

Membrane protein fractionation. A crude membrane protein fraction from parental CHO, 5-HT_{2A}R–CHO, or 5-HT_{2C}R–CHO cells was used to assess the specificity of the 5-HT_{2C}R–PTEN association via coimmunoprecipitation (co-IP) and Western blotting techniques as described previously (Anastasio et al., 2010). Cells were rinsed and scraped in ice-cold Krebs' solution (in mM: 125 NaCl, 1.2 KCl, 1.2 $MgSO_4$, 1.2 $CaCl_2$, 22 Na_2CO_3, 1 NaH_2PO_4, and 10 glucose), centrifuged at 800 × *g* for 2 min to pellet the cells, and resuspended and homogenized in 200 μl of extraction buffer [10 mM HEPES, 1 mM EDTA, 2 mM EGTA, 1 mM DTT, protease inhibitor cocktail (10 μl/ml; Sigma), and phosphatase inhibitor cocktails 2 and 3 (10 μl/ml each; Sigma)]. After differential centrifugation, the membrane-enriched pellet was washed once and then resuspended in 200 μl of resuspension buffer (20 mM HEPES, 400 mM NaCl, 1 mM EDTA, 1 mM EGTA, 1 mM DTT, protease and phosphatase inhibitors, and 0.5% NP-40).

A crude membrane protein fraction from rat brain was used to assess peptide disruption of the 5-HT_{2C}R–PTEN complex *in vivo*. The ventral tegmental area (VTA) was homogenized in 10 times w/v extraction buffer as described above. The homogenate was centrifuged at 1000 × *g* for 10 min at 4°C to pellet the nuclear fraction. The supernatant was removed and centrifuged at 20,000 × *g* at 4°C for 30 min to pellet the membrane-bound protein fraction. The membrane-enriched pellet was washed once and then resuspended in 200 μl of resuspension buffer (20 mM HEPES, 400 mM NaCl, 1 mM EDTA, 1 mM EGTA, 1 mM DTT, protease and phosphatase inhibitors, and 0.5% dodecyl maltoside).

Immunoprecipitation (IP) assays. The 5-HT_2R or PTEN antibodies (45 or 10 μg/reaction, respectively) were covalently crosslinked onto protein A/G resin according to the instructions of the manufacturer (Pierce Crosslink Immunoprecipitation Kit; Pierce Biotechnology) and as de-

scribed previously (Anastasio et al., 2010). Precleared membrane protein (400–500 μg) was incubated with the antibody-crosslinked resin overnight at 4°C with constant shaking. The suspension was centrifuged at 1000 × *g* for 30 s, and the bound antigen–antibody-crosslinked resin was washed twice with IP lysis/wash buffer and then once with 1× conditioning buffer. The bound complex was incubated for 5 min at room temperature in elution buffer (Pierce Crosslink Immunoprecipitation Kit); the eluted antigen was subjected to cold acetone precipitation, and the protein sample was centrifuged at 15,000 × *g* for 10 min at 4°C. The acetone was decanted, and the precipitated protein was resuspended in 2× loading buffer and subjected to SDS-PAGE. Immunoblotting (IB) for 5-HT_2R and PTEN was performed as described below.

Immunoblotting. Total protein concentration was determined with the BCA assay (Pierce Biotechnology). Equal amounts of protein were reduced with Laemmli's sample buffer, heated for 20 min at 70°C, then separated by SDS-PAGE using 4–12% Bis-Tris gels (Invitrogen) for 2–3 h at 110 V. After gel electrophoresis, proteins were transferred to a PVDF membrane (Bio-Rad) via a wet-transfer electroblotting apparatus (Bio-Rad) overnight at 60 V (Anastasio et al., 2010). Western blot assays were conducted as follows: membranes were blocked with Odyssey blocking buffer [1:1 in Tris-buffered saline (TBS), pH 7.4; LI-COR Biosciences] for 1 h, followed by incubation with primary antibody overnight. Membranes were rinsed three time for 10 min in TBS plus 0.1% Tween 20 (TBS-T), incubated with secondary antibody for 45 min, then rinsed three times for 10 min in TBS-T. Immunoreactive bands were detected with the Odyssey Infrared Imaging System (LI-COR Biosciences).

Antibodies. Primary antibodies included the following: mouse monoclonal 5-HT_{2C}R (D-12, C-terminus epitope, 1:100, sc-17797; Santa Cruz Biotechnology); mouse monoclonal PTEN (04-035, C-terminus epitope, 1:1000; Millipore); rabbit polyclonal PTEN (07-1372, C-terminus epitope, 1:500; Millipore); and rabbit polyclonal 5-HT_{2A}R (RA24288, N-terminus epitope, 1:100; Neuromics). Secondary antibodies (used at 1:10,000 for 1 h at room temperature) included the following: infrared-labeled goat anti-mouse (IRDye680, 926-32220; LI-COR Biosciences); goat anti-rabbit (IRDye800, 827-08365; LI-COR Biosciences); donkey anti-goat (IRDye800CW, 605-731-125; Rockland Immunochemicals); and sheep anti-mouse (IRDye680; Rockland Immunochemicals). For the Duolink proximity ligation assay (PLA), two proprietary, species-specific secondary antibodies conjugated to short DNA strands were used [PLA probe anti-mouse MINUS (92004-100) and PLA probe anti-rabbit PLUS (92002-0100; Olink Bioscience)].

Data analyses. PVDF membranes were imaged using the Odyssey Infrared Imaging System (LI-COR Biosciences) at 700 and/or 800 nm at 169 μm resolution. The integrated intensity of each band was analyzed with the Odyssey Infrared Imaging System Application version 2.1 software. The ratio of the sample immunoreactive band intensity to β-actin immunoreactive band intensity was determined for normalization. A one-way ANOVA using the general linear model (GLM) procedure (SAS for Windows, version 9.3; SAS Institute) was used to assess differences in the density of 5-HT_{2C}R–PTEN protein expression. A priori comparisons of the effects of 3L4F were conducted using Dunnett's procedure, with vehicle as the comparator. The α level for all analyses was set at $p < 0.05$.

Duolink PLA. Immunocytochemical localization of 5-HT_{2C}R–PTEN complexes was established via the Duolink PLA with a 5-HT_{2C}R antibody raised to an epitope at the C terminus in mouse (Abbas et al., 2009; Anastasio et al., 2010), a PTEN antibody raised to an epitope at the C terminus in rabbit (Müller et al., 2011) and species-specific secondary antibodies conjugated to short DNA strands (see above). This assay was conducted in 5-HT_{2C}R–CHO cells grown on coverslips, as described above. The Duolink PLA was performed according to the recommended protocol of the manufacturer with minor modifications. Cellular plasma membrane glycoproteins and glycolipids of live cells were labeled with fluorescent wheat germ agglutinin according to the protocol of the manufacturer (Invitrogen). Cells were then pretreated with vehicle (HBSS) or 1 pM 3L4F (15 min) and rapidly washed 2× in ice-cold Dulbecco's PBS (DPBS) and fixed in cold 4% paraformaldehyde (30 min). After fixation, cells were washed three times with DPBS, permeabilized with 0.25% Triton X-100 (15 min), and then washed three times with DPBS. Coverslips were incubated with 3% normal donkey serum for 1 h to block nonspecific antibody binding, followed by primary antibodies to 5-HT_{2C}R (1:250) and PTEN (1:500) in 3% normal donkey serum overnight at 4°C. Coverslips were mounted onto slides with DAPI-containing medium.

The Duolink PLA signals were quantified from photomicrographs (Trifilieff et al., 2011) obtained with a Carl Zeiss LSM-510 META confocal microscope [100×, 1.40 numerical aperture oil-immersion objective (University of Texas Medical Branch Optical Microscopy Core, Galveston, TX)] after excitation at 364 and 543 nm with two different channels of emission with sequential acquisition. After excitation at 364 nm, emission was measured with a 385–470 nm filter; excitation at 543 nm emission was measured with a 560–615 nm filter. The *Z*-stack acquisition was performed at *Z*-steps of 0.3 μm. All images were collected using eight-frame Kallman averaging with a pixel time of 1.26 μs, voxel size of 120 × 120 × 60 nm, and a frame size of 1024 × 1024 pixels.

Data analyses. Images were captured from a minimum of four fields of view [~20–30 cells throughout the entire *z*-axis (20–30 planes per field of view)] per coverslip (two independent coverslips per condition). The rendering and quantification of Duolink PLA signals was calculated using automatic threshold and classification based on intensity and size of the spots (Imaris 7.0 Bitplane Scientific, Andor Technology). The number of Duolink PLA signals was normalized to DAPI-positive nuclei (Trifilieff et al., 2011). The effects of 3L4F were compared with vehicle by a Student's *t* test (SAS for Windows); α level set at $p < 0.05$.

Functional analyses of the 5-HT_{2C}R–PTEN interaction in vitro

Intracellular calcium assay. Changes in intracellular calcium (Ca_i^{2+}) release were determined using the calcium-sensitive dye Calcium 4 (R8142; Molecular Devices) according to previously published protocols (Shashack et al., 2011; Ding et al., 2012; Seitz et al., 2012). Cells were plated in serum-replete medium at indicated densities in black-sided, clear-bottom 96-well tissue culture plates. Cells were fed 24 h later with serum-free medium, and, after overnight incubation, medium was removed and replaced with 80 μl of Calcium 4 dye solution dissolved in HBSS and supplemented with 2.5 mM water-soluble probenicid to inhibit transport of the dye to the outside of the cell. Plates were returned to the 37°C incubator for 60 min and then incubated for an additional 60 min at room temperature in the dark.

Fluorescence was measured with a FlexStation3 (Molecular Devices). The experiment started with establishment of baseline for 17 s after addition of vehicle (HBSS without calcium or magnesium). Addition of 5-HT [1 nM (approximate EC_{50}) for 5-HT_{2C}R–CHO cells or 10 nM (approximate EC_{50}) for 5-HT_{2A}R–CHO cells] or 20 nM WAY163909 (approximate EC_{50}) for 5-HT_{2C}R–CHO cells occurred at the 17 s time point, and fluorescence was recorded every 1.7 s for 90–120 s (Shashack et al., 2011; Ding et al., 2012; Seitz et al., 2012). To assess the effects of 3L4F on the concentration–response relationship for 5-HT in 5-HT_{2C}R–CHO cells, addition of 5-HT (10 pM to 1 μM) occurred at the 17 s time point, and fluorescence was recorded every 1.7 s for 90–120 s (Shashack et al., 2011; Ding et al., 2012; Seitz et al., 2012). Preincubation with vehicle (HBSS), 3L4F peptide, or 3L4F peptide fragments occurred 15 min before the start of the experiment. Maximum peak height was determined by the FlexStation software (SoftMax Pro 5.2).

Data analyses. Peak responses from each well were normalized to total cell mass as determined with crystal violet staining and then expressed as a percentage of the "control" Ca_i^{2+} response obtained with 1 nM 5-HT or 20 nM WAY163909 for 5-HT_{2C}R–CHO cells or 10 nM 5-HT for 5-HT_{2A}R–CHO cells (Shashack et al., 2011; Ding et al., 2012; Seitz et al., 2012). For 5-HT fold-shift analyses, peak responses from each well were normalized to total cell mass as determined with crystal violet staining and then expressed as a percentage of the maximum Ca_i^{2+} response obtained with 100 nM 5-HT in 5-HT_{2C}R–CHO cells. Comparisons to analyze the effects of compounds on Ca_i^{2+} release were defined before the start of experiment; therefore, one-way repeated-measures ANOVA (SAS for Windows) and a priori comparisons of the treatment means versus control were made with Dunnett's procedure (peptide concentration–response curves) or Student's *t* test comparing the response at each 5-HT concentration with that in the presence of 1 pM 3L4F (5-HT fold-shift curve); α level was set at $p < 0.05$.

Functional analyses of the 5-HT$_{2C}$R–PTEN interaction in vivo

Animals. Male Sprague Dawley rats (Harlan) weighing 225–325 g at the start of the experiments were used ($n = 60$). Rats were allowed to acclimate for 5–7 d in a colony room at a constant temperature (21–23°C) and humidity (45–50%) on a 12 h light/dark cycle (lights on 7:00 A.M. to 7:00 P.M.). For co-IP studies, rats were anesthetized (chloral hydrate solution, 400 mg/kg) and decapitated, and the brain was microdissected immediately on a cool tray (4°C) (Heffner et al., 1980; Liu et al., 2007; Anastasio et al., 2010). Samples were flash frozen in liquid nitrogen and stored at −80°C for subsequent protein extraction. For locomotor studies, rats were housed four rats per cage with food and water *ad libitum* throughout all phases of the studies. For one-choice serial reaction time (1-CSRT) task training, rats were housed two per cage and food restricted to 90% of free-feeding weight for the duration of all experiments; water was available *ad libitum* except during daily 30–60 min operant sessions. All experiments were performed in accordance with the National Institutes of Health *Guide for the Care and Use of Laboratory Animals* and with the approval of the University of Texas Medical Branch Institutional Animal Care and Use Committee.

Locomotor activity. Locomotor activity was monitored and quantified under low-light conditions using a modified open-field activity system (San Diego Instruments) according to previous publications with minor modifications (Cunningham et al., 2011). Clear Plexiglas chambers (40 × 40 × 40 cm) were surrounded by a 4 × 4 photobeam matrix positioned 4 cm from the chamber floor. Consecutive photobeam breaks within the 16 × 16 cm of the activity monitor were recorded as central ambulation. Peripheral ambulation was counted as consecutive beam breaks in the surrounding perimeter. Central and peripheral ambulations were summed to provide a measure of total horizontal ambulation. Vertical activity (i.e., rearing) was captured using a row of 16 photobeams positioned 16 cm from the activity monitor floor. Rats ($n = 20$) were acclimated to the colony room, and, after 1 week of handling, rats were habituated to the activity monitors for 30 min. The effects of rat TAT–3L4F alone or in combination with the selective 5-HT$_{2C}$R agonist WAY163909 were established in a within-subjects design. To control for order effects, drug doses and vehicles were administered in random sequence to individual rats across sessions such that all rats received all treatment combinations and were tested every 3 d. On each test day, rats received vehicle (1 ml/kg saline, i.p.), rat TAT–3L4F (0.1 or 1 μmol/kg, i.p.), or the combination of rat TAT–3L4F (0.1 μmol/kg, i.p.) plus WAY163909 (1 mg/kg, i.p.) 15 min before placement in activity monitors; locomotor activity was assessed for 70 min. The combination of rat TAT–3L4F plus WAY163909 was administered simultaneously.

1-CSRT task. The effects of the rat TAT–3L4F, the selective 5-HT$_{2C}$R agonist WAY163909, or the combination of both on impulsive action were assessed in the 1-CSRT task as described previously (Anastasio et al., 2011; Cunningham et al., 2012). The 1-CSRT task is a variant of the 5-CSRT task (Dalley et al., 2002; Winstanley et al., 2004a; Anastasio et al., 2011; Cunningham et al., 2012) and provides information concerning the ability to withhold a prepotent response, a measure of impulsive action. In the 1-CSRT task, reinforcement is earned for the detection and correct responding to a brief visual stimulus presented regularly in a spatially predictable location. The 1-CSRT task procedures took place in standard five-hole nose-poke operant chambers (Med Associates) contained within a ventilated and sound-attenuating chamber. Each chamber was fitted with an array of five evenly spaced response apertures (2.5 × 2.5 × 2.2 cm) positioned 2 cm above a bar floor, and each aperture contained a stimulus light. Nose-poke responses into these apertures were detected by a horizontally positioned infrared beam located 1 cm from the entrance to each hole. The chambers are also fitted on the opposite wall with a house light, food tray, and an external pellet dispenser capable of delivering 45 mg pellets (Dustless Precision pellets; Bio-Serv). The chambers were connected via an interface (Med Associates) to a personal computer running Med PC for Windows software (Med Associates) that controlled and recorded all experimental events.

1-CSRT task training. Rats ($n = 32$) were allowed 1 week to acclimate to the colony after which food restriction began. Rats were weighed daily to ensure that body weights were maintained at 90% of free-feeding levels throughout 1-CSRT task training. Training began with a pretraining stage in which the rat was habituated to the test chamber and introduced to nose-poke responding for food pellets. During this stage, all responses made in the correctly lit (center) hole resulted in the illumination of the magazine light and presentation of a single food pellet. The training stages thereafter each comprised daily sessions of 100 trials to be completed in a maximum of 30 min; each training stage involved incrementally lowering the stimulus duration with a 5 s limited hold and an intertrial interval (ITI) of 5 s. Thus, a maximum of 100 correct responses in a session would result in a maximum of 100 reinforcers delivered; incorrect or premature responses or omissions resulted in a 5 s timeout period and a reduction in potential reinforcers obtained. Rats were required to meet an acquisition criteria of a minimum of 50 correct responses, >80% accuracy [correct responses/(correct + incorrect) × 100], and <20% omissions (omitted responses/trials completed × 100) to move from one training stage to the next (for details, see Anastasio et al., 2011).

Pharmacological test sessions commenced after animals met the stable training criteria of >80% accuracy and <20% omissions for five consecutive training sessions on the final training stage (0.5 s stimulus duration, 5 s limited hold, 5 s ITI) with <15% variability across sessions. Pretreatment with (1) vehicle (0.9% saline, i.p.), (2) WAY163909 (0.05, 0.1, 0.2, 0.1, and 1 mg/kg, i.p), (3) rat TAT–3L4F (0.3 μmol/kg, i.p.), or (4) rat TAT–3L4F (0.3 μmol/kg, i.p.) plus WAY163909 (0.1 mg/kg) occurred 15 min before the start of the 1-CSRT task session. The combination of rat TAT–3L4F plus WAY163909 was administered simultaneously.

Data analyses. Locomotor activity data are presented as mean total horizontal ambulation, total vertical activity, peripheral ambulation, or central ambulation (± SEM) over the entire 70 min session or within 5 min time bins across the session. A two-way ANOVA for repeated measures for the factors of treatment and time was conducted. The main effect of treatment on total horizontal ambulation, total vertical activity, peripheral ambulation, and central ambulation was analyzed with a repeated-measures, one-way ANOVA using the GLM procedure (SAS for Windows). Subsequent a priori comparisons between means for total horizontal ambulation, total vertical activity, peripheral ambulation, and central ambulation were made using the Dunnett's procedure, with vehicle (saline) as the comparator. During the 1-CSRT task, the total number of responses (correct, incorrect, omissions, and premature) as well as the latency to start the task (seconds), time to finish (minutes), and reinforcer latency (time to retrieve reinforcer; minutes) were recorded. Incorrect responses consistently accounted for <5% of total responses during 1-CSRT task test sessions because rats were well trained. Percentage accuracy was used as an indication of the attentional capacity of each rat. Percentage omissions indicated the motivation level of each rat to perform the task. Responses during the ITI (premature responses) and the number of reinforcers earned during the 1-CSRT task were used to measure impulsive action. Responses on pharmacological test sessions are presented as the percentage of values observed on the training session 1 d before the pharmacological test session; before this session, rats were injected with saline (control). Because group comparisons were specifically defined before the start of the experiment, preplanned comparisons were conducted after an overall F test in a multifactorial ANOVA (Keppel, 1973). Thus, comparisons to analyze the effects of TAT–3L4F, WAY163909, and TAT–3L4F plus WAY163909 on percentage accuracy, percentage omissions, time to start, time to finish, reinforcer latency, premature responses, and reinforcers earned were subjected to a one-way repeated-measures ANOVA, and a priori comparisons of the treatment means versus saline were made with Dunnett's procedure (SAS for windows); α level for all analyses was set to $p < 0.05$.

Results

A 16 aa segment of the third intracellular loop of the human 5-HT$_{2C}$R (3L4F; Pro280–Arg295; Fig. 1) represents a "hotspot" interface for the 5-HT$_{2C}$R–PTEN interaction (Ji et al., 2006; Tesmer, 2006). A BLAST search of the sequence for 3L4F revealed significant alignment ($E < 1$) only with the 5-HT$_{2C}$R across several species. Of importance, the sequence for 3L4F was not aligned with 5-HT$_{2A}$R or 5-HT$_{2B}$R, thus reducing the possibility that the third intracellular loop of these receptors form a complex with PTEN. The synthesized rat 3L4F peptide, when preapplied

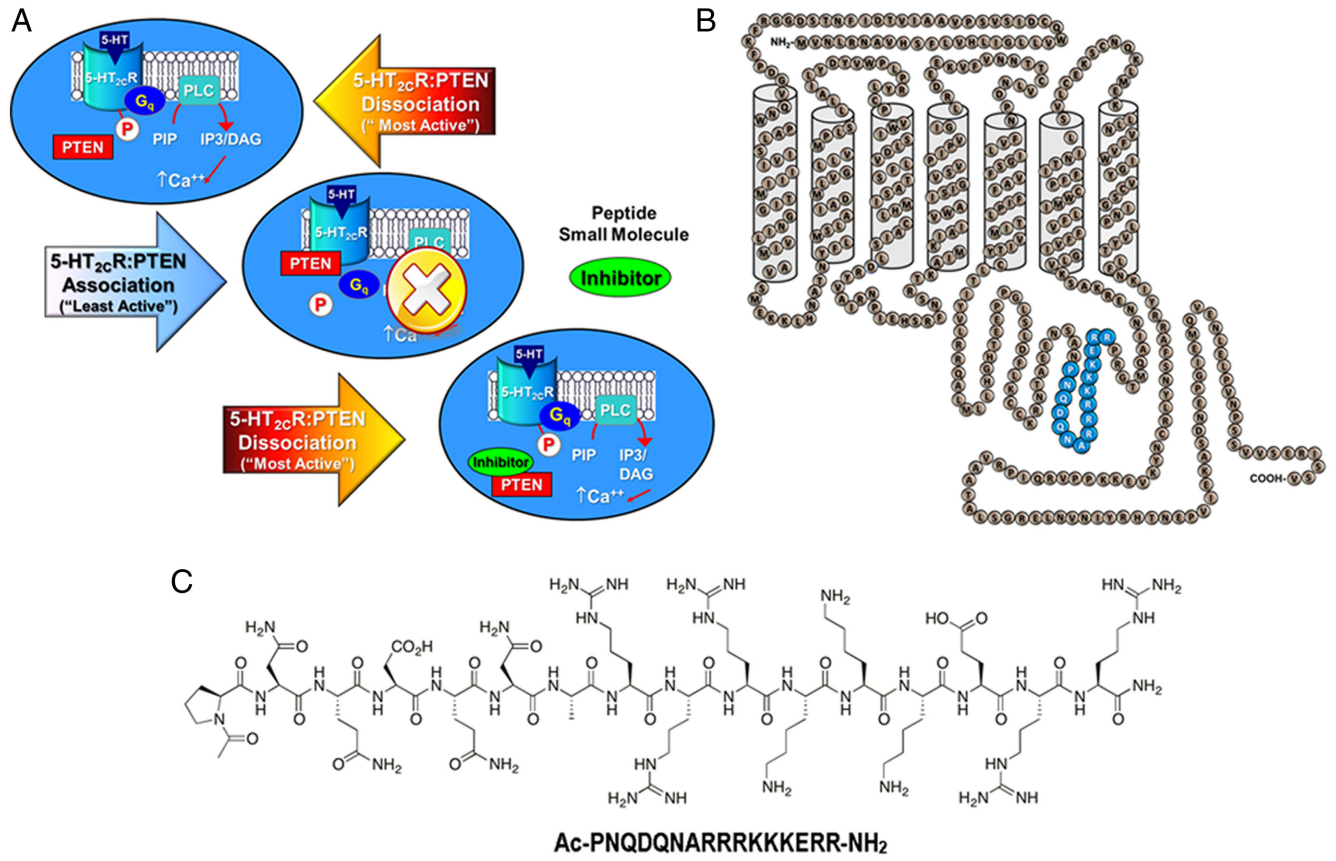

Figure 1. Disruption of the 5-HT$_{2C}$R–PTEN complex is predicted to result in positive allosteric modulation of 5-HT$_{2C}$R signaling. ***A***, Signaling through 5-HT$_{2C}$R is proposed to be "most active" under conditions of 5-HT$_{2C}$R stimulation and dissociation of the third intracellular loop of the 5-HT$_{2C}$R from PTEN (top). Association of 5-HT$_{2C}$R with PTEN is predicted to limit 5-HT$_{2C}$R signaling (middle). A peptide fragment of the 5-HT$_{2C}$R (3L4F) (or a potential small molecule) is proposed to compete with 5-HT$_{2C}$R for binding to PTEN (bottom) to enhance 5-HT$_{2C}$R signaling (adapted from Ji et al., 2006). ***B***, A schematic representation of the human 5-HT$_{2C}$R protein (adapted from Julius et al., 1988, 1989) illustrates predicted amino acid residues (Pro280 –Arg295) of 5-HT$_{2C}$R that bind PTEN (blue). ***C***, The chemical structure of PTEN and its amino acid content is presented.

to PC12 lysates, blocked co-IP of PTEN with 5-HT$_{2C}$R and prevented PTEN-mediated dephosphorylation of the 5-HT$_{2C}$R protein in PC12 cells, an outcome linked to the protein phosphatase (not lipid phosphatase) actions of PTEN (Ji et al., 2006). These provocative findings suggest that 5-HT$_{2C}$R signaling (Fig. 1*A*, top) may be allosterically modulated such that the association of PTEN with the third intracellular loop of the 5-HT$_{2C}$R protein limits 5-HT$_{2C}$R signaling (Fig. 1*A*, middle). The 3L4F peptide fragment (Fig. 1 *B*, *C*) is proposed to disrupt 5-HT$_{2C}$R binding to PTEN (Fig. 1*A*, bottom) (Ji et al., 2006) and would be predicted to promote 5-HT$_{2C}$R downstream signaling.

Physical analyses of 5-HT$_{2C}$R–PTEN interaction *in vitro*

We used co-IP and Duolink PLA to investigate the physical association between 5-HT$_{2C}$R and PTEN in a cellular model appropriate to examine the role of the 5-HT$_{2C}$R–PTEN complex in 5-HT$_{2C}$R-mediated signaling in live cells. The 5-HT$_{2C}$R–CHO cells express native PTEN, and the downstream signaling events evoked by stimulation of the 5-HT$_{2C}$R are well characterized in these cells (Berg et al., 2001; Stout et al., 2002; Gavarini et al., 2006; Moya et al., 2007; Seitz et al., 2012). We also used CHO cells stably transfected with the homologous 5-HT$_{2A}$R (Shashack et al., 2011; Ding et al., 2012; Seitz et al., 2012) to investigate the specificity of the observations noted in the 5-HT$_{2C}$R–CHO cells.

Immunoprecipitation of membrane protein extracts of 5-HT$_{2C}$R–CHO cells using the 5-HT$_{2C}$R antibody followed by IB with the PTEN antibody yields a band at the expected molecular weight (MW) (55 kDa) for PTEN (Fig. 2*A*, 0 time point); the reciprocal experiment (PTEN IP followed by 5-HT$_{2C}$R IB) yields a band at the expected MW (46 kDa) for 5-HT$_{2C}$R (data not shown). These results confirm that the complex with 5-HT$_{2C}$R occurs under basal conditions with native levels of PTEN in 5-HT$_{2C}$R–CHO cells. We also incubated live 5-HT$_{2C}$R–CHO cells with 1 pM 3L4F for 0, 5, or 15 min [concentration based on optimization and published data (Ji et al., 2006)]. Preincubation with the 3L4F peptide reduced the intensity of the PTEN immunoreactive band detected after IP for the 5-HT$_{2C}$R in a time-dependent manner (Fig. 2*A*). A main effect of time on expression of the complex was observed ($F_{(2,15)} = 7.23$, $p < 0.05$; Fig. 2*B*); a priori comparisons revealed that 1 pM 3L4F at 15 min significantly reduced the formation of the 5-HT$_{2C}$R–PTEN complex versus the 0 min time point after IP for 5-HT$_{2C}$R and IB for PTEN in 5-HT$_{2C}$R–CHO cells ($p < 0.05$). IB for 5-HT$_{2C}$R after IP for 5-HT$_{2C}$R indicates that comparable levels of 5-HT$_{2C}$R protein were immunoprecipitated across time after 3L4F treatment (Fig. 2*A*). These data suggest that the 3L4F peptide rapidly and potently disrupts the 5-HT$_{2C}$R–PTEN interaction in 5-HT$_{2C}$R–CHO cells. This outcome was not attributable to alterations in absolute membrane protein expression levels of either 5-HT$_{2C}$R or PTEN, which were unchanged after preincubation with 1 pM 3L4F for 15 min (Fig. 2*C*).

A similar experiment was conducted in 5-HT$_{2A}$R–CHO cells to determine whether 5-HT$_{2A}$R formed a protein complex with PTEN. Figure 2*D* shows that IP with the 5-HT$_{2A}$R antibody followed by IB with the PTEN antibody did not yield an immuno-

reactive band for PTEN either with or without preincubation with 3L4F (1 pM); the reciprocal experiment (PTEN IP followed by 5-HT$_{2A}$R IB) did not yield an immunoreactive band for 5-HT$_{2A}$R (data not shown). IB for 5-HT$_{2A}$R after IP for 5-HT$_{2A}$R indicates that comparable levels of 5-HT$_{2A}$R membrane protein were immunoprecipitated across treatment conditions (Fig. 2*D*). Furthermore, the 3L4F peptide did not alter 5-HT$_{2A}$R or PTEN membrane protein expression levels in 5-HT$_{2A}$R–CHO cells (Fig. 2*E*). Protein expression levels in both the 5-HT$_{2A}$R–CHO and 5-HT$_{2C}$R–CHO cells have been assessed at ~200 fmol/mg protein, which approximates physiological levels in brain (Berg et al., 1998). Thus, the lack of association of 5-HT$_{2A}$R with PTEN is not attributable to differences in expression levels of 5-HT$_{2A}$R relative to the 5-HT$_{2C}$R in these cell lines and indicates that 5-HT$_{2A}$R and PTEN do not form a protein complex. These data support the results of a BLAST analysis that showed that the 3L4F peptide shared homology with the 5-HT$_{2C}$R across species but not with 5-HT$_{2A}$R or any other known proteins.

The formation of the 5-HT$_{2C}$R–PTEN complex was demonstrated to occur in co-IP studies of lysates from the rat VTA *ex vivo* (Ji et al., 2006). We have also identified the complex in membrane fractions of the rat VTA (Fig. 2*F*) and medial prefrontal cortex (our unpublished observations). Here, IP of VTA membrane protein fractions using the 5-HT$_{2C}$R antibody followed by IB with the PTEN antibody yields a band at the expected MW for PTEN, indicating the presence of the 5-HT$_{2C}$R–PTEN complex in the VTA (Fig. 2*F*) (Ji et al., 2006). In rats administered the rat TAT–3L4F peptide systemically (10 μmol/kg, i.p.) and killed 5 min later, the intensity of the PTEN immunoreactive band detected after IP for the 5-HT$_{2C}$R was attenuated relative to vehicle (saline) treatment (Fig. 2*F*). IB for 5-HT$_{2C}$R after IP for 5-HT$_{2C}$R indicates that comparable levels of 5-HT$_{2C}$R protein were immunoprecipitated from VTA samples extracted from vehicle-treated and rat TAT–3L4F-treated rats (Fig. 2*F*). These data demonstrate for the first time that systemic administration of the rat TAT–3L4F peptide *in vivo* disrupts expression of the 5-HT$_{2C}$R–PTEN complex in the VTA.

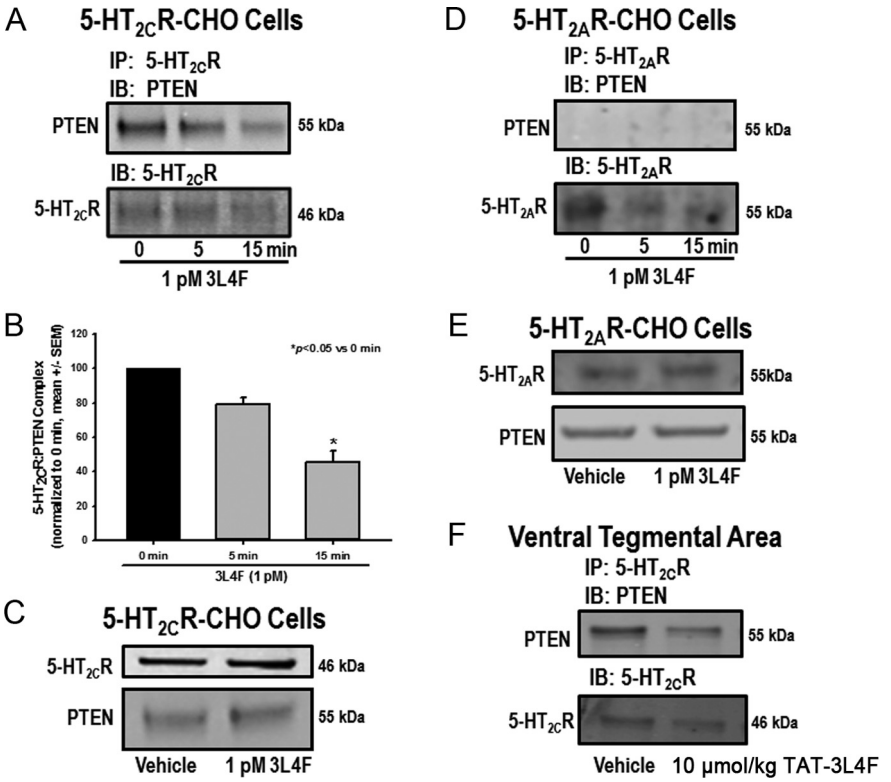

Figure 2. The 3L4F peptide disrupts the complex between 5-HT$_{2C}$R and PTEN in 5-HT$_{2C}$R–CHO cells and rat brain. 5-HT$_{2C}$R and PTEN are part of a protein complex in 5-HT$_{2C}$R–CHO cells and rat brain as demonstrated on co-IP. The 5-HT$_{2C}$R–PTEN complex is effectively disrupted by the small peptide fragment 3L4F, which competes with PTEN for binding to 5-HT$_{2C}$R. The 5-HT$_{2C}$R–CHO cells were incubated with 3L4F (1 pM) for 0, 5, or 15 min. ***A***, ***B***, Qualitative (***A***) and quantitative (***B***) data demonstrate that preincubation with 3L4F reduced the intensity of the PTEN band in a time-dependent manner after IP for 5-HT$_{2C}$R. ***C***, Preincubation with 1 pM 3L4F (15 min) did not alter protein expression levels of 5-HT$_{2C}$R or PTEN in 5-HT$_{2C}$R–CHO cells as assessed by Western blot. ***D***, To assess specificity for 5-HT$_{2C}$R over the highly homologous 5-HT$_{2A}$R, IP for 5-HT$_{2A}$R followed by IB for PTEN was conducted in 5-HT$_{2A}$R–CHO cells. The PTEN immunoreactive band was not observed, indicating that 5-HT$_{2A}$R did not associate with PTEN in 5-HT$_{2A}$R–CHO cells. ***E***, The 3L4F peptide did not alter 5-HT$_{2A}$R or PTEN protein expression levels in 5-HT$_{2A}$R–CHO cells as assessed by Western blot. ***F***, IP of protein extracts from the VTA using the 5-HT$_{2C}$R antibody followed by IB with the PTEN antibody yields a band at the expected MW (55 kDa) for PTEN, indicating the presence of the 5-HT$_{2C}$R–PTEN complex in the VTA (Ji et al., 2006). The rat TAT–3L4F peptide (10 μmol/kg, i.p., 5 min treatment) reduced the intensity of the PTEN immunoreactive band detected after IP for 5-HT$_{2C}$R relative to vehicle (saline) treatment. *$p < 0.05$ versus 0 min.

We used a well-characterized PLA (Duolink PLA) (Söderberg et al., 2006; Trifilieff et al., 2011; Watson et al., 2012) to corroborate the co-IP studies and to detect whether the protein complex in 5-HT$_{2C}$R–CHO cells can be disrupted by the 3L4F peptide *in situ*. Oligonucleotides ligated to the two secondary antibodies hybridize and if in close proximity (<40 nM) to the DNA strands linked to the secondary antibodies ligate to become a primer for a rolling-circle amplification incorporating fluorescent nucleotides; a concatemeric product is generated and visualized as a single red fluorescent spot. Figure 3 illustrates such 5-HT$_{2C}$R–PTEN complexes in the 5-HT$_{2C}$R–CHO cells. The 5-HT$_{2C}$R–PTEN complex formation was not detected when one or the other of the primary antibodies was omitted (data not shown). Figure 3*A* is a low-power magnification photomicrograph that illustrates the expression of the 5-HT$_{2C}$R–PTEN complex (red spots) in 5-HT$_{2C}$R–CHO cells; cellular membranes are labeled with wheat germ agglutinin (green), and the nuclei are labeled with DAPI (blue). Representative images from the reconstruction of confocal images were selected (Fig. 3*A*, white box), and progressive rotation of the *Z*-stack in the *y* direction illustrates the distribution of the 5-HT$_{2C}$R–PTEN complex throughout the cell (Fig. 3*B*). To better identify the subcellular localization pattern of the 5-HT$_{2C}$R–PTEN complex, a photomicrograph was prepared from a confocal series of 5-HT$_{2C}$R–CHO cells sectioned tangentially (Fig. 3*C*). Orthogonal views demonstrate that 5-HT$_{2C}$R–PTEN complexes are clearly evident in the *x*–*z* and *y*–*z* directions relative to the image plane (Fig. 3*C*). The 5-HT$_{2C}$R–PTEN complex appears to form prominently in plasma membrane and/or cytoplasmic compartments (Fig. 3*C*). In concordance with our co-IP results, 1 pM 3L4F (15 min) reduced the number of 5-HT$_{2C}$R–PTEN complexes observed with the Duolink PLA relative to vehicle control (Fig. 3*D*). There was a significant reduction in the number of

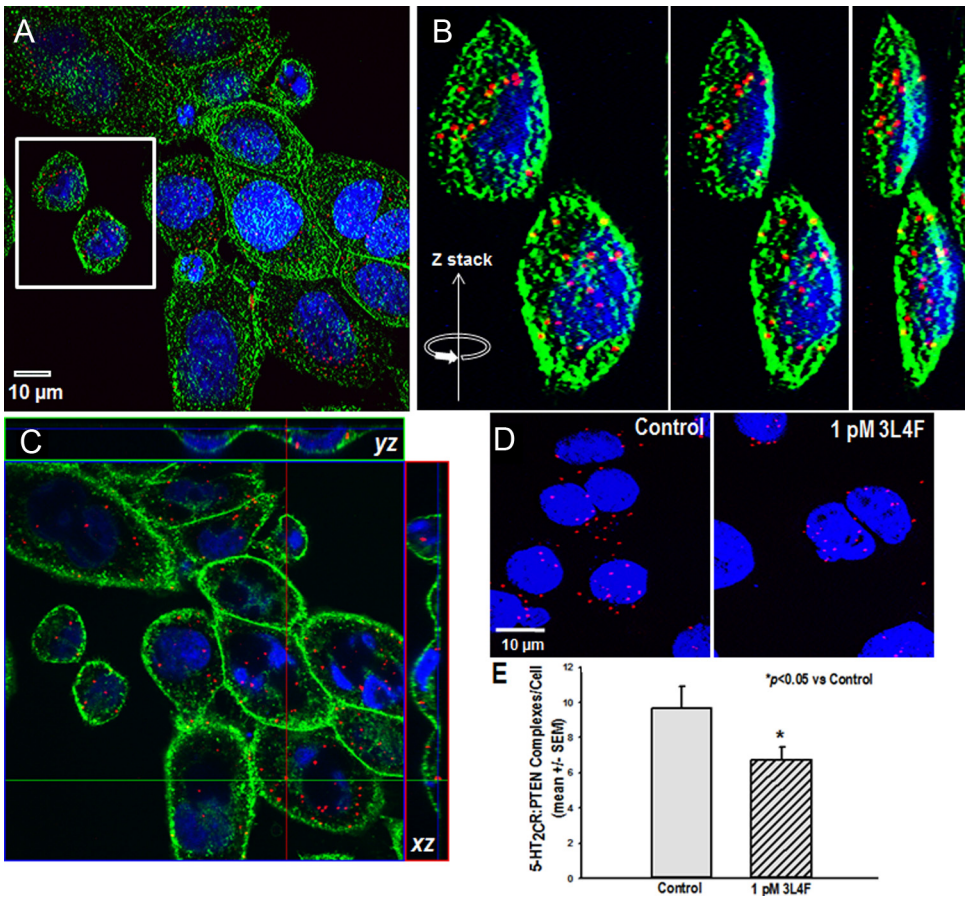

Figure 3. The 5-HT$_{2C}$R–PTEN complex is observed and 3L4F disrupts its assembly in live cells *in situ*. ***A–D***, Representative photomicrographs of 5-HT$_{2C}$R–PTEN complexes as measured by the Duolink PLA in the 5-HT$_{2C}$R–CHO cells. ***A***, Confocal reconstruction of the 5-HT$_{2C}$R–PTEN complex (red spots) in 5-HT$_{2C}$R–CHO cells; the cellular membrane is labeled with wheat germ agglutinin (green), and the nucleus is labeled with DAPI (blue). ***B***, Representative images from the reconstruction of confocal images were selected (***A***, white box), and progressive rotation of the *Z*-stack in the *y* direction illustrates the distribution of the 5-HT$_{2C}$R–PTEN complex throughout the cell. ***C***, Photomicrograph prepared from a confocal series of 5-HT$_{2C}$R–CHO cells sectioned tangentially. Orthogonal views indicate that 5-HT$_{2C}$R–PTEN complexes are clearly evident in the *x–z* and *y–z* directions relative to the image plane. The 5-HT$_{2C}$R–PTEN complex appears to form prominently in plasma membrane and/or cytoplasmic compartments. ***D***, ***E***, Qualitative (***D***) and quantitative (***E***) representation demonstrating significant disruption of the number of 5-HT$_{2C}$R–PTEN complexes by the 3L4F peptide (1 pM; 15 min) relative to control. *$p < 0.05$ versus control.

5-HT$_{2C}$R–PTEN Duolink PLA complexes per cell in the presence of 1 pM 3L4F ($p < 0.05$; Fig. 3*E*). These data indicate that the formation of the 5-HT$_{2C}$R–PTEN complex occurs under native conditions within intact cells and is not an artifact of *in vitro* processing for biochemical analysis. Together, we identified the assembly of the 5-HT$_{2C}$R–PTEN complex and its disruption by 3L4F specifically in live 5-HT$_{2C}$R–CHO, but not 5-HT$_{2A}$R–CHO, cells; thus, these cellular models provide an appropriate means through which to study the impact of the complex on downstream signaling.

Functional analyses of 5-HT$_{2C}$R–PTEN interaction *in vitro*

Intracellular calcium release was quantified in 5-HT$_{2C}$R–CHO cells to determine the functional consequence of 5-HT$_{2C}$R–PTEN complex formation in live cells. Evaluation of the efficacy of 3L4F to impact signaling through the 5-HT$_{2C}$R was conducted using the EC_{50} (1 nM) for 5-HT to evoke Ca_i^{2+} release in 5-HT$_{2C}$R–CHO cells to allow detection of potential allosteric modulation in this key component of downstream 5-HT$_{2C}$R signaling (Shashack et al., 2011; Ding et al., 2012; Seitz et al., 2012). Although preincubation with the 3L4F peptide (15 min) did not alter unstimulated Ca_i^{2+} release ($F_{(6,28)} = 0.58$, NS; Fig. 4*A*), a main effect of 3L4F treatment was observed for 5-HT-evoked Ca_i^{2+} release ($F_{(6,26)} = 4.23$, $p < 0.05$; Fig. 4*B*); a priori comparisons revealed that concentrations of 10^{-12} to 10^{-9} M 3L4F significantly increased Ca_i^{2+} release versus 1 nM 5-HT ($p < 0.05$; Fig. 4*B*). In a separate experiment, the maximal 5-HT-evoked Ca_i^{2+} release (determined by analysis of the 5-HT concentration response) was significantly potentiated in the presence of 1 pM (15 min) 3L4F (E_{max} = 120.7% of maximal response for 5-HT; $p < 0.05$).

The TAT peptide was conjugated to the N terminus of the rat 3L4F peptide to foster cell penetrability of the 3L4F peptide (Schwarze et al., 1999; Aarts et al., 2002), and rat TAT–3L4F was first tested in the cellular models to determine efficacy relative to the human 3L4F peptide. A concentration-dependent increase in 5-HT-induced Ca_i^{2+} release in 5-HT$_{2C}$R–CHO cells was seen for the rat TAT–3L4F ($F_{(6,28)} = 4.03$, $p < 0.05$; Fig. 4*B*); no effect of the rat TAT–3L4F on Ca_i^{2+} release was observed when tested alone (data not shown). A priori comparisons demonstrated that concentrations of 10^{-13} to 10^{-10} M rat TAT–3L4F significantly elevated Ca_i^{2+} release versus 1 nM 5-HT ($p < 0.05$; Fig. 4*B*). We evaluated the specificity of the 3L4F peptide for 5-HT$_{2C}$R versus 5-HT$_{2A}$R signaling. In contrast to observations in the 5-HT$_{2C}$R–CHO cells, the 3L4F peptide did not potentiate 5-HT-mediated (10 nM) Ca_i^{2+} release (Fig. 4*C*) nor did it alter Ca_i^{2+} release when tested alone (data not shown) in 5-HT$_{2A}$R–CHO cells. Thus, both the human 3L4F peptide and the rat TAT–3L4F peptide efficaciously enhanced 5-HT$_{2C}$R downstream signaling, but there is no indication

that either peptide alters signaling through 5-HT$_{2A}$R. Observations of the efficacy of the 3L4F peptide to potentiate 5-HT$_{2C}$R signaling evoked by its endogenous ligand were then extended to the selective 5-HT$_{2C}$R agonist WAY163909 (Dunlop et al., 2006; Rosenzweig-Lipson et al., 2006; Cunningham et al., 2011). After preincubation with the 3L4F peptide, we observed a dose-dependent increase in WAY163909-evoked (20 nM) Ca_i^{2+} release ($F_{(6,13)} = 8.28$, $p < 0.05$; Fig. 4*D*); a priori comparisons revealed that concentrations of 10^{-12} to 10^{-8} M 3L4F significantly increased Ca_i^{2+} release versus 20 nM WAY163909 ($p < 0.05$; Fig. 4*D*). Together, these data indicate that the 3L4F peptide allosterically augments the activation of downstream signaling evoked by either the native ligand or a synthetic full 5-HT$_{2C}$R agonist.

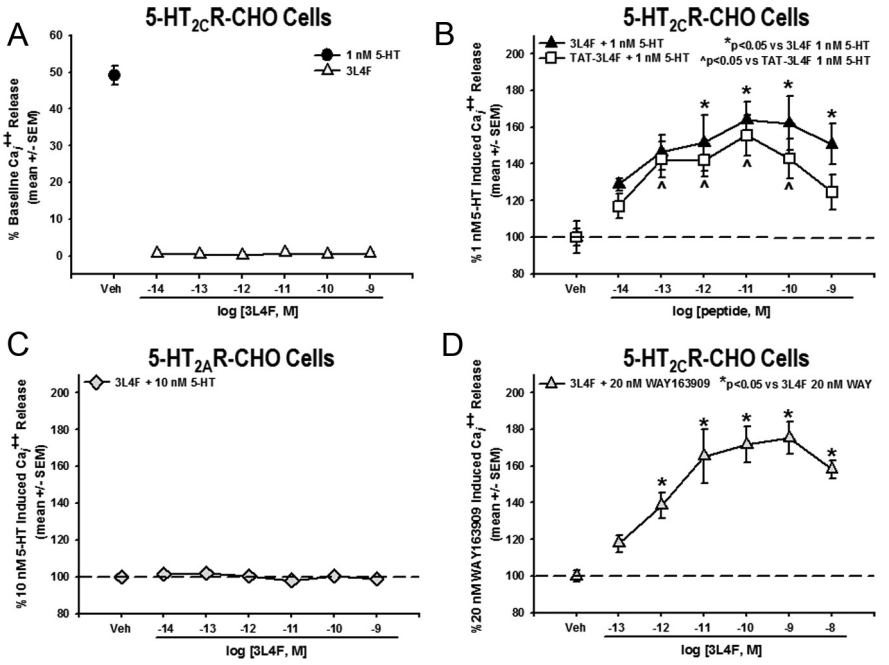

Figure 4. The 3L4F peptide enhances 5-HT-induced Ca_i^{2+} release in 5-HT$_{2C}$R–CHO cells. ***A***, Preincubation with the 3L4F peptide alone (15 min; △) did not induce Ca_i^{2+} release in the 5-HT$_{2C}$R–CHO cells. The EC_{50} for 5-HT-mediated Ca_i^{2+} release is 1 nM in 5-HT$_{2C}$R–CHO cells (●). ***B***, Preincubation with 3L4F (15 min) dose dependently (10^{-12} to 10^{-9} M) increased Ca_i^{2+} release versus 1 nM 5-HT-evoked Ca_i^{2+} release in the 5-HT$_{2C}$R–CHO cells (*$p < 0.05$ vs 1 nM 5-HT; ▲). Preincubation with rat TAT–3L4F (15 min) dose dependently (10^{-13} to 10^{-10} M) increased Ca_i^{2+} release versus 1 nM 5-HT-evoked Ca_i^{2+} release in the 5-HT$_{2C}$R–CHO cells (^$p < 0.05$ vs 1 nM 5-HT; □). ***C***, Preincubation with the 3L4F peptide alone (15 min) did not induce Ca_i^{2+} release in the 5-HT$_{2A}$R–CHO cells. ***D***, Preincubation with 3L4F (15 min) dose dependently (10^{-12} to 10^{-8} M) increased the 5-HT$_{2C}$R-selective agonist WAY163909-evoked (20 nM) Ca_i^{2+} release in the 5-HT$_{2C}$R–CHO cells (*$p < 0.05$ vs 20 nM WAY163909; △). Veh, Vehicle.

Functional analyses of 5-HT$_{2C}$R–PTEN interaction *in vivo*

The 5-HT$_{2C}$R–PTEN complex has been identified in the rat VTA (Ji et al., 2006) (Fig. 2*F*) and medial prefrontal cortex (our unpublished observations), key nuclei of the limbic–corticostriatal circuitry critical in attention, motivation, cognition, and reward processes (Bechara et al., 2001; Goldstein et al., 2007; Bubar and Cunningham, 2008). Furthermore, the initial *in vivo* profile of TAT–3L4F in rats is consistent with behavioral effects mediated through activation of 5-HT$_{2C}$R (Ji et al., 2006). In the present study, we directly evaluated the efficacy of rat TAT–3L4F to alter multiple measures of motor activity as well as affect performance in the operant 1-CSRT task that indexes impulsivity and cognitive function in rodents (Dalley et al., 2002; Robbins, 2002; Winstanley et al., 2004a; Anastasio et al., 2011; Cunningham et al., 2012).

Several 5-HT$_{2C}$R agonists are reported to suppress both horizontal ambulation and vertical (rearing) activity (Halford et al., 1997; Grottick et al., 2000; Fletcher et al., 2002; Halberstadt et al., 2009; Cunningham et al., 2011, 2012). Here, we assessed the effects of rat TAT–3L4F peptide (0.1 or 1 μmol/kg) on outcome measures obtained from analyses of spontaneous locomotor activity; the doses chosen for systemic administration were based on a previous behavioral analysis (Ji et al., 2006) and our preliminary studies (unpublished observations). A main effect of treatment ($F_{(2,447)} = 5.84$, $p < 0.05$) and time ($F_{(13,447)} = 174.23$, $p < 0.05$), but no treatment × time interaction ($F_{(26,447)} = 1.35$, NS), was observed for horizontal ambulation divided into 5-min bins (Fig. 5*A*). TAT–3L4F at 1 μmol/kg significantly reduced horizontal ambulation versus saline at 5, 10, and 15 min ($p < 0.05$; Fig. 5*A*). A main effect of TAT–3L4F treatment was observed for total horizontal ambulation totaled across the 70 min test session ($F_{(2,31)} = 5.84$, $p < 0.05$; Fig. 5*A*, inset); a priori comparisons revealed that 1 μmol/kg TAT–3L4F significantly reduced total horizontal ambulation versus saline ($p < 0.05$; Fig. 5*A*, inset). No main effect of treatment ($F_{(2,447)} = 1.48$, NS), time ($F_{(13,447)} = 94.85$, $p < 0.05$), or treatment × time interaction ($F_{(26,447)} = 0.54$, NS) was observed for vertical activity divided into 5-min intervals (Fig. 5*B*). No main effect of TAT–3L4F versus saline was observed for vertical activity totaled across the 70 min test session ($F_{(2,31)} = 1.48$, NS; Fig. 5*B*, inset).

Horizontal ambulation in the peripheral versus central field of the activity monitor was evaluated to assist in the choice of a dose to be used in analyses of allosteric regulation of the 5-HT$_{2C}$R *in vivo*. A main effect of treatment ($F_{(2,433)} = 6.79$, $p < 0.05$), time ($F_{(13,433)} = 175.05$, $p < 0.05$), and a trend toward a treatment × time interaction ($F_{(26,433)} = 1.44$, $p = 0.07$) was observed for peripheral ambulation divided into 5-min bins (Fig. 5*C*). A priori comparisons indicated that TAT–3L4F (1 μmol/kg) significantly reduced peripheral ambulation versus saline at 5 and 10 min ($p < 0.05$; Fig. 5*C*). A main effect of TAT–3L4F treatment was observed for peripheral ambulation totaled across the 70 min test session ($F_{(2,31)} = 7.45$, $p < 0.05$; Fig. 5*C*, inset); TAT–3L4F (1 μmol/kg) significantly reduced peripheral ambulation versus saline ($p < 0.05$; Fig. 5*C*, inset). No main effect of treatment ($F_{(2,447)} = 2.42$, NS), time ($F_{(13,447)} = 80.64$, $p < 0.05$), or treatment × time interaction ($F_{(26,447)} = 1.18$, NS) was observed for central ambulation divided into 5-min bins (Fig. 5*D*). No main effect of TAT–3L4F treatment was observed for central ambulation ($F_{(2,31)} = 2.42$, NS; Fig. 5*D*, inset) totaled across the 70 min test session (Fig. 5*D*, inset). Thus, these data indicate that the highest tested dose of TAT–3L4F (1 μmol/kg) induced a behavioral profile in rats consistent with agonist actions at the 5-HT$_{2C}$R (Cunningham et al., 2011).

The fine-grained analysis of motor activity (above) allowed identification of 0.1 μmol/kg TAT–3L4F as ineffective across multiple activity measures and supports the use of this TAT–3L4F dose for analyses of allosteric effects *in vivo*. Figure 6 illustrates the allosteric effects of rat TAT–3L4F peptide (0.1 μmol/

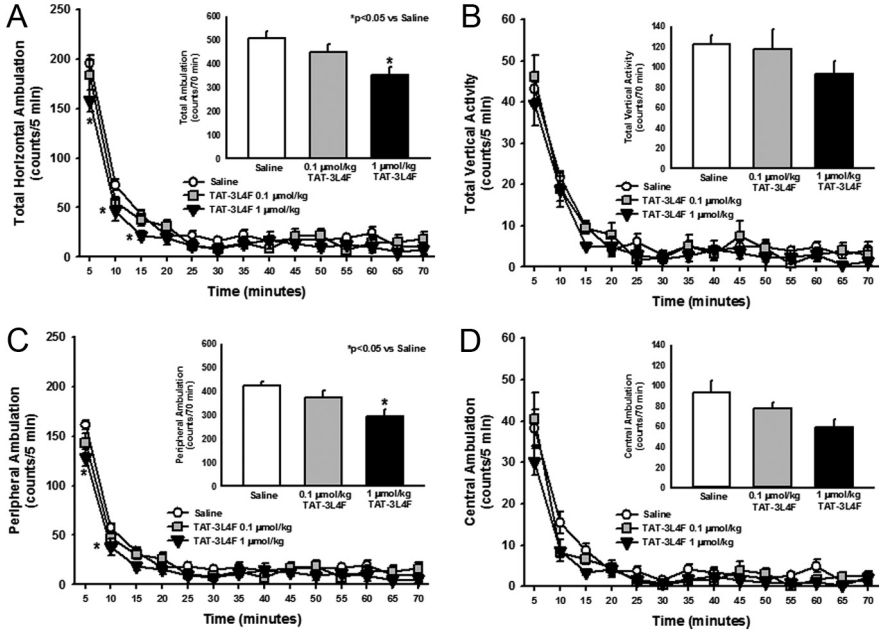

Figure 5. The TAT–3L4F peptide suppresses ambulation but not vertical activity. We assessed the effects of saline (1 ml/kg, i.p.) or rat TAT–3L4F peptide (0.1 or 1 μmol/kg, i.p.) on spontaneous locomotor activity. ***A***, The time course of horizontal ambulation is divided into 5 min time bins across the 70 min session; TAT–3L4F at 1 μmol/kg significantly reduced horizontal ambulation versus saline during the first 15 min. ***A***, Inset, The mean ± SEM total horizontal ambulation is represented after administration of saline or TAT–3L4F; TAT–3L4F (1 μmol/kg) significantly reduced total horizontal ambulation versus saline. ***B***, The time course of vertical activity is divided into 5 min time bins across the 70 min session. ***B***, Inset, the mean ± SEM total vertical activity is represented after administration of saline or TAT–3L4F. ***C***, The time course of peripheral ambulation is divided into 5 min time bins across the 70 min session; TAT–3L4F (1 μmol/kg) significantly reduced peripheral ambulation versus saline during the first 10 min. ***C***, Inset, The mean ± SEM total peripheral ambulation is represented after administration of saline or TAT–3L4F; TAT–3L4F (1 μmol/kg) significantly reduced peripheral ambulation versus saline. ***D***, The time course of central ambulation is divided into 5 min time bins across the 70 min session. ***D***, Inset, The mean ± SEM total central ambulation is represented after administration of saline or TAT–3L4F. *$p < 0.05$ versus saline.

kg) in combination with the selective 5-HT$_{2C}$R agonist WAY163909 (1 mg/kg) on spontaneous locomotor activity. A main effect of treatment ($F_{(3,643)} = 3.08$, $p < 0.05$) or time ($F_{(13,643)} = 114.39$, $p < 0.05$), but no treatment × time interaction ($F_{(39,643)} = 1.05$, NS), was observed for horizontal ambulation divided into 5-min bins (Fig. 6*A*). A priori comparisons indicated that neither TAT–3L4F nor WAY163909 at the chosen dose altered horizontal ambulation versus saline at any 5 min interval (NS; Fig. 6*A*), as predicted by our previous observations (Cunningham et al., 2011, 2012). Furthermore, the combination of TAT–3L4F plus WAY163909 did not significantly alter horizontal ambulation versus saline at any specific 5-min interval (NS; Fig. 6*A*). However, a main effect of treatment was observed for horizontal ambulation totaled across the 70 min test session ($F_{(3,45)} = 3.08$, $p < 0.05$; Fig. 6*A*, inset); a priori comparisons revealed that, although neither ligands tested alone at chosen doses altered total horizontal ambulation, the combination of TAT–3L4F plus WAY163909 significantly reduced total horizontal ambulation versus saline ($p < 0.05$; Fig. 6*A*, inset). No main effect of treatment ($F_{(3,629)} = 1.27$, NS), time ($F_{(13,629)} = 95.61$, $p < 0.05$), or treatment × time interaction ($F_{(39,629)} = 0.84$, NS) was observed for vertical activity divided into 5-min intervals (Fig. 6*B*). No main effect of treatment was observed for vertical activity totaled across the 70 min test session ($F_{(3,44)} = 1.27$, NS; Fig. 6*B*, inset). A main effect of treatment ($F_{(3,643)} = 3.4$, $p < 0.05$), time ($F_{(13,643)} = 304.63$, $p < 0.05$), and a treatment × time interaction ($F_{(39,643)} = 1.69$, $p < 0.05$) was observed for peripheral ambulation divided into 5-min bins (Fig. 6*C*). A priori comparisons indicated that WAY163909 and the combination of TAT–3L4F plus WAY163909 significantly reduced peripheral ambulation versus saline at 5 and 10 min ($p < 0.05$; Fig. 6*C*). A main effect of treatment was observed for peripheral ambulation totaled across the 70 min test session ($F_{(3,45)} = 3.4$, $p < 0.05$; Fig. 6*C*, inset); the combination of TAT–3L4F plus WAY163909, but not either ligand alone, significantly reduced peripheral ambulation versus saline ($p < 0.05$; Fig. 6*C*, inset). A main effect of treatment ($F_{(3,643)} = 3.35$, $p < 0.05$) and time ($F_{(13,643)} = 107.84$, $p < 0.05$), but no treatment × time interaction ($F_{(39,643)} = 1.3$, NS), was observed for central ambulation divided into 5-min bins (Fig. 6*D*). A priori comparisons indicated that WAY163909 and the combination of TAT–3L4F plus WAY163909 significantly reduced central ambulation versus saline at 10 min ($p < 0.05$; Fig. 6*D*). A main effect of treatment was observed for central ambulation ($F_{(3,447)} = 3.35$, $p < 0.05$; Fig. 6*D*, inset) totaled across the 70 min test session; the combination of TAT–3L4F plus WAY163909, but not either ligand alone, significantly reduced central ambulation versus saline ($p < 0.05$; Fig. 6*D*, inset). These data demonstrate that the TAT–3L4F peptide augments selective 5-HT$_{2C}$R agonist-mediated suppression of spontaneous locomotor activity.

Selective 5-HT$_{2C}$R agonists, including WAY163909 (Navarra et al., 2008), potently suppress (Winstanley et al., 2004a; Fletcher et al., 2007) whereas selective 5-HT$_{2C}$R antagonists (e.g., SB242084) increase impulsive action assessed by premature (anticipatory) responses in the 5-CSRT task (Winstanley et al., 2004b; Fletcher et al., 2007). We established the 1-CSRT task (Dalley et al., 2002; Winstanley et al., 2004a; Anastasio et al., 2011) to allow pharmacological analyses of impulsive action under conditions of reduced visuospatial attentional processes (Dalley et al., 2002; Winstanley et al., 2004a; Anastasio et al., 2011; Cunningham et al., 2012). Rats were trained to criterion on the 1-CSRT task, and we first evaluated the efficacy of our reference 5-HT$_{2C}$R agonist WAY163909, followed by an analysis of TAT–3L4F to alter impulsivity alone or in combination with a low dose of WAY163909. Rats met criterion for acquisition of the 1-CSRT task in 33 ± 0.8 d. Figure 7 displays the number of premature responses (Fig. 7*A*) and reinforcers earned (Fig. 7*B*) for each dose of WAY163909 tested; data are presented as a percentage of the number of premature responses made on the saline administration session (control) that preceded each dose evaluated. A main effect of WAY163909 dose on premature responses ($F_{(5,212)} = 4.96$, $p < 0.05$) was observed; a priori comparisons showed that 0.5 and 1 mg/kg WAY163909 decreased premature responses versus saline ($p < 0.05$; Fig. 7*A*, dashed line indicates saline levels). A main effect of WAY163909 dose on the number of reinforcers earned ($F_{(5,212)} = 3.73$, $p < 0.05$) was observed; a priori comparisons showed that 0.5 and 1 mg/kg WAY163909 increased the number of reinforcers earned versus saline ($p < 0.05$; Fig. 7*B*, dashed line indicates saline levels). Descriptive sta-

tistics for percentage accuracy ($F_{(5,212)} = 1.46$, NS), percentage omissions ($F_{(5,212)} = 1.25$, NS), latency to start ($F_{(5,212)} = 1.59$, NS), time to finish ($F_{(5,212)} = 0.88$, NS), and reinforcer latency (time to retrieve reinforcer after a correct response ($F_{(5,212)} = 0.70$, NS) in the 1-CSRT task for saline and each dose of WAY163909 administered are presented in Table 1. Thus, these data extend a previous study in the 5-CSRT task (Navarra et al., 2008) to demonstrate efficacy of WAY163909 in the 1-CSRT task and support a key role for 5-HT$_{2C}$R activation in normalizing impulsive action.

We then analyzed TAT–3L4F (0.3 μmol/kg) either alone or in combination with a dose (0.1 mg/kg) of WAY163909 that was ineffective in the 1-CSRT task. Figure 7 displays the number of premature responses (Fig. 7*C*) and reinforcers earned (Fig. 7*D*) for TAT–3L4F, WAY163909, or the combination; data are presented as a percentage of the number of responses made on the saline administration session that preceded each dose evaluated. A main effect of treatment on premature responses ($F_{(3,49)} = 4.15$, $p < 0.05$) was observed; a priori comparisons showed that TAT–3L4F (0.3 μmol/kg) plus WAY163909 (0.1 mg/kg) significantly decreased premature responses versus saline ($p < 0.05$; Fig. 7*C*, dashed line indicates saline levels). Neither 0.3 μmol/kg TAT–3L4F nor 0.1 mg/kg WAY163909 alone altered premature responses (NS; Fig. 7*C*, dashed line indicates saline levels). A main effect of treatment on the number of reinforcers earned ($F_{(3,49)} = 3.50$, $p < 0.05$) was observed; a priori comparisons showed TAT–3L4F plus WAY163909 increased the number of reinforcers earned versus saline ($p < 0.05$; Fig. 7*D*, dashed line indicates saline levels). Neither 0.3 μmol/kg TAT–3L4F nor 0.1 mg/kg WAY163909 alone altered the number of reinforcers earned versus saline (NS; Fig. 7*D*, dashed line indicates saline levels). Descriptive statistics for percentage accuracy ($F_{(3,49)} = 1.07$, NS), percentage omissions ($F_{(3,49)} = 0.49$, NS), latency to start ($F_{(3,49)} = 1.84$, NS), time to finish ($F_{(3,49)} = 2.75$, NS), and reinforcer latency ($F_{(3,49)} = 2.50$, NS) in the 1-CSRT task for vehicle, TAT–3L4F alone, WAY163909 alone, and the combination of TAT–3L4F plus WAY163909 administration are presented in Table 2. Thus, TAT–3L4F and WAY163909 synergize to attenuate impulsive action consistent with positive allosteric modulation of 5-HT$_{2C}$R function.

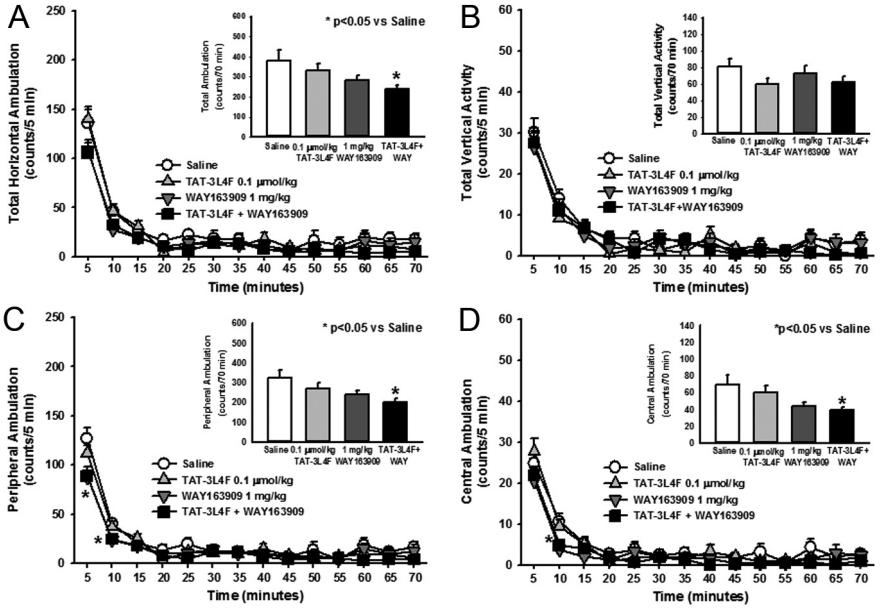

Figure 6. The combination of TAT–3L4F plus the selective 5-HT$_{2C}$R agonist WAY163909 suppresses ambulation but not vertical activity. We assessed the effects of saline (1 ml/kg, i.p.), rat TAT–3L4F peptide (0.1 μmol/kg, i.p.), or the combination of TAT–3L4F plus WAY163909 (1 mg/kg, i.p.) on spontaneous locomotor activity. ***A***, The time course of horizontal ambulation is divided into 5 min time bins across the 70 min session. ***A***, Inset, The mean ± SEM total horizontal ambulation is represented after administration of saline, TAT–3L4F, or TAT–3L4F plus WAY163909; TAT–3L4F plus WAY163909 significantly reduced total horizontal ambulation versus saline. ***B***, The time course of vertical activity is divided into 5 min time bins across the 70 min session. ***B***, Inset, The mean ± SEM total vertical activity is represented after administration of saline, TAT–3L4F, or TAT–3L4F plus WAY163909. ***C***, The time course of peripheral ambulation is divided into 5 min time bins across the 70 min session; WAY163909 alone and TAT–3L4F plus WAY163909 significantly reduced peripheral ambulation versus saline during the first 10 min. ***C***, Inset, The mean ± SEM total peripheral ambulation is represented after administration of saline, TAT–3L4F, or TAT–3L4F plus WAY163909; TAT–3L4F plus WAY163909 significantly reduced peripheral ambulation versus saline. ***D***, The time course of central ambulation is divided into 5 min time bins across the 70 min session; WAY163909 and TAT–3L4F plus WAY163909 significantly reduced central ambulation versus saline at the 10 min time point. ***D***, Inset, The mean ± SEM total central ambulation is represented after administration of saline, TAT–3L4F, or TAT–3L4F plus WAY163909; TAT–3L4F plus WAY163909 significantly reduced central ambulation versus saline. *$p < 0.05$ versus saline.

Identification of active fragments of 3L4F

The 3L4F peptide demonstrated efficacy and specificity to disrupt the 5-HT$_{2C}$R–PTEN complex both *in vitro* and *in vivo*. The next step was to generate new peptides based on the backbone of 3L4F to establish the residues of the peptide responsible for the observed interaction with PTEN. Three overlapping fragments of the 3L4F peptide (3L4F-F$_1$, 3L4F-F$_2$, and 3L4F-F$_3$) were synthesized and evaluated for efficacy in the Ca_i^{2+} release assay in 5-HT$_{2C}$R–CHO (and 5-HT$_{2A}$R–CHO) cells. Preincubation with the 3L4F-F$_1$, 3L4F-F$_2$, or 3L4F-F$_3$ alone (15 min) did not induce Ca_i^{2+} release (data not shown). A main effect of 3L4F-F$_1$ treatment was observed for 5-HT-evoked Ca_i^{2+} release ($F_{(6,28)} = 7.94$, $p < 0.05$; Fig. 8*A*); a priori comparisons revealed that concentrations of 10^{-13} to 10^{-9} M 3L4F-F$_1$ significantly increased Ca_i^{2+} release versus 1 nM 5-HT ($p < 0.05$; Fig. 8*A*). No main effect of 3L4F-F$_2$ ($F_{(6,19)} = 2.23$, NS; Fig. 8*B*) or 3L4F-F$_3$ treatment was observed for 5-HT-evoked Ca_i^{2+} release ($F_{(6,14)} = 0.35$, NS; Fig. 8*C*). In the 5-HT$_{2A}$R–CHO cells, preincubation with the 3L4F-F$_1$, 3L4F-F$_2$, or 3L4F-F$_3$ peptide alone (15 min) did not induce Ca_i^{2+} release or alter Ca_i^{2+} release evoked by 10 nM 5-HT (data not shown). Thus, the active fragment of 3L4F is a component of the first 8 aa of the peptide (3L4F-F$_1$).

We then mapped the contact residues between the 3L4F or 3L4F-F$_1$ peptides and PTEN to investigate the interaction interface and to evaluate the secondary structural content of the peptides. REMD simulation runs were performed to assess the predominant 3L4F (Fig. 9*A*) and 3L4F-F$_1$ (Fig. 9*B*,*C*) conformation populations and secondary structure. Visual analyses of the 3L4F peptide trajectories revealed a majority of β-turn-like structures with some amount of α-helical content at the N terminus (Fig. 9*A*). The dPCA analysis of the 300,000 REMD trajectory of the 3L4F-F$_1$ peptide revealed α-helical content (Fig. 9*B*) correlated to the same N-terminus region as 3L4F (Fig. 9*A*), whereas the primary two α-helical subconformations of the 3L4F-F$_1$ peptide differ in the presence or absence of an Arg8–Asp4 (R8–D4) salt bridge (Fig. 9*B*). Additional analysis of the 300,000 REMD trajectory of the 3L4F-F$_1$ peptide revealed that the third highest populated

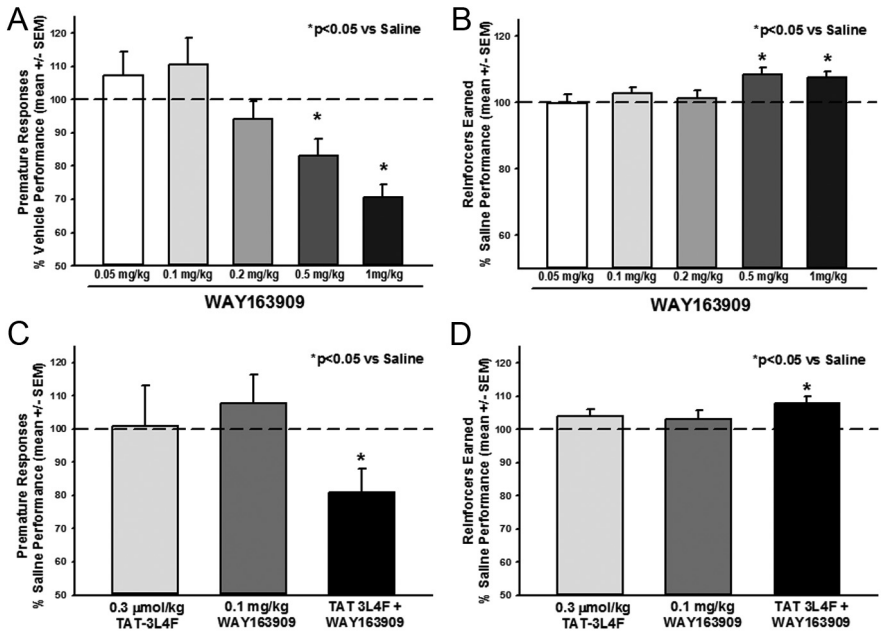

Figure 7. The selective 5-HT$_{2C}$R agonist WAY163909 alone or in combination with TAT–3L4F suppresses impulsive action in the 1-CSRT task. WAY163909 (0.05, 0.1, 0.2, 0.5, and 1 mg/kg) was administered 15 min before saline injections; 1 ml/kg saline was administered immediately before 1-CSRT task test sessions in a counterbalanced within-subjects design. Data are presented as a percentage of the number of responses made on the saline administration session that preceded each dose evaluated. ***A***, ***B***, WAY163909 (0.5 and 1 mg/kg, i.p.) decreased premature responses (***A***) and increased the number of reinforcers earned (***B***) versus saline. The combination effects of the rat TAT–3L4F peptide (0.03 μmol/kg) plus WAY163909 (0.1 mg/kg) on impulsive action indices in the 1-CSRT task were evaluated. The combination of TAT–3L4F plus WAY163909 administered 15 min before saline injections (1 ml/kg saline was administered immediately before 1-CSRT task test sessions in a between-subjects design) significantly altered impulsive action in the 1-CSRT task. ***C***, ***D***, TAT–3L4F plus WAY163909 decreased premature responses (***C***) and increased the number of reinforcers earned (***D***) versus saline. Neither WAY163909 (0.1 mg/kg) nor TAT–3L4F (0.3 μmol/kg) alone altered the number of premature responses (***C***) or reinforcers earned (***D***). *$p < 0.05$ versus saline (dashed line indicates saline levels).

Table 1. 1-CSRT task descriptive statistics (mean ± SEM) for WAY163909 administration

Treatment	% Accuracy	% Omissions	Latency to start (s)	Time to finish (s)	Response latency (s)
Saline	100.48 ± 0.4	5.94 ± 0.7	1.11 ± 0.2	919.57 ± 15.2	2.40 ± 0.2
WAY163909 (mg/kg)					
0.05	100.52 ± 0.4	6.23 ± 1.1	0.69 ± 0.2	933.62 ± 29.4	2.75 ± 0.4
0.1	100.72 ± 0.5	5.40 ± 0.9	1.13 ± 0.2	923.55 ± 16.5	2.57 ± 0.2
0.2	100.15 ± 0.7	6.26 ± 1.6	0.85 ± 0.2	941.12 ± 34.9	2.84 ± 0.4
0.5	100.61 ± 0.4	5.85 ± 0.9	0.62 ± 0.1	926.23 ± 17.3	2.54 ± 0.2
1	101.48 ± 0.6	8.94 ± 0.7	1.11 ± 0.2	981.14 ± 33.7	3.06 ± 0.4

Table 2. 1-CSRT task descriptive statistics (mean ± SEM) for WAY163909 plus TAT–3L4F administration

Treatment	% Accuracy	% Omissions	Latency to start (s)	Time to finish (s)	Response latency (s)
Saline	99.92 ± 0.4	4.32 ± 1.9	0.62 ± 0.2	864.08 ± 21.6	2.14 ± 0.3
TAT–3L4F 0.3 μmol/kg	98.69 ± 0.6	4.77 ± 1.0	1.00 ± 0.6	875.10 ± 15.3	2.19 ± 0.2
WAY163909 0.1 mg/kg	100.21 ± 0.8	5.45 ± 1.0	1.11 ± 0.3	948.78 ± 37.7	2.83 ± 0.5
WAY163909 plus TAT–3L4F	98.99 ± 0.8	2.42 ± 0.8	2.72 ± 1.3	1000.73 ± 56.3	3.96 ± 0.8

structure was a β-turn (Fig. 9*C*). Next, we performed coarse-grained docking between the 3L4F-F$_1$ peptide and the surface of the PTEN protein using GRAMM (Fig. 9*D*,*E*). α-Helical 3L4F-F$_1$ conformations were shown to cluster primarily in the central groove between the phosphatase active site and C2 membrane-targeting structural domain of the PTEN crystal structure (Fig. 9*D*). A secondary, less populated cluster site was found on the immediately opposite side of the central groove (Fig. 9*E*). GRAMM docking of β-turn conformations yields similar results (data not shown).

We then used CD analysis of protein conformations to experimentally evaluate the secondary structure of the 3L4F (Fig. 9*F*) and 3L4F-F1 (Fig. 9*G*) as well as to compare these results to the REMD simulation predictions. Data are presented as three independent trials. CD analysis of α-helical structures has a characteristic negative signal at 222 nm (Chen et al., 1974). The 3L4F peptide (300 μM) has a clear inflection point at 222 nm, although the overall contribution of the α-helix is <50% (Fig. 9*F*). The 3L4F-F$_1$ peptide (100 and 300 μM) retains a shallow inflection point at 222 nm, indicating 10–30% α-helical populations (Fig. 9*G*). These CD experimental results complement the REMD simulations (Fig. 9*B*,*C*) in which both α-helix and loop conformations were populated in the ensemble of trajectories. On the whole, these data suggest that the secondary structural elements of 3L4F-F$_1$ are important for PTEN recognition and inhibition. The structure–activity relationships that have been developed with the 3L4F peptide derivatives will be used to design small-molecule scaffolds that possess the same or better activity than the 3L4F-F$_1$ peptide and also display the important pharmacophores in the same spatial orientation as predicted by molecular dynamic modeling.

Discussion

Serotonergic neurotransmission via 5-HT$_{2C}$R in limbic–corticostriatal circuits has been implicated as a critical mechanism involved in a number of chronic pathological maladies. At present, very little is known about the coordinated formation of protein–protein interactions that regulate 5-HT$_{2C}$R signaling under normal and dysfunctional states in these neural circuits. We discovered that the close physical association of 5-HT$_{2C}$R with PTEN serves as a new allosteric regulatory mechanism to control 5-HT$_{2C}$R-mediated biology based on convergent cellular and behavioral data. We have also identified the active fragment of 3L4F as a component of an 8 aa span of the third intracellular loop of 5-HT$_{2C}$R (Pro280–Arg287). These compelling data demonstrate the specificity and importance of this protein assembly in cellular events and behavior. These data also propose a chemical guidepost for the future development of drug-like peptide or small-molecule inhibitors as neuroprobes to study 5-HT$_{2C}$R allostery and develop therapeutics for 5-HT$_{2C}$R-mediated disorders.

The third intracellular loop of 5-HT$_{2C}$R is critically important in G-protein selectivity and activation (Cheung et al., 1992), and we present the first demonstration that a peptide derived from this loop is functionally important to 5-HT$_{2C}$R-mediated signaling in live cells. Both the human 3L4F and rat TAT–3L4F peptides

enhanced orthosteric ligand-mediated signaling through 5-HT$_{2C}$R. Importantly, the 3L4F peptide did not alter 5-HT$_{2A}$R signaling, indicating specificity for modulation of 5-HT$_{2C}$R function. Thus, PTEN selectively controls the 5-HT$_{2C}$R signalosome, and 3L4F disrupts this association, resulting in allosteric augmentation of downstream signaling evoked by either the native ligand or a synthetic 5-HT$_{2C}$R agonist.

Association of PTEN with the third intracellular loop of 5-HT$_{2C}$R interferes with agonist-induced phosphorylation of 5-HT$_{2C}$R (Ji et al., 2006), an action that has been reported to prevent receptor desensitization and promote resensitization processes (Backstrom et al., 2000). Because the functional effects of 3L4F to enhance 5-HT$_{2C}$R signaling are dependent on ligand activation of the receptor (present studies) and the phosphorylation state of the receptor (Ji et al., 2006), the peptide may promote resensitization mechanisms that "protect" against functional tolerance to maintain activation of the 5-HT$_{2C}$R by agonists. Furthermore, our multiple approaches showed that the magnitude of this allosteric potentiation is saturable, as expected for blockade of an interaction site by a peptide. This suggests that fine-tuning of the orthosteric site-activated intracellular signaling is possible, potentially dampening the negative consequences of extended 5-HT$_{2C}$R activation (e.g., desensitization) (Keov et al., 2011; Melancon et al., 2012). Because PTEN coupling appears to predict 5-HT$_{2C}$R signaling strength, disruption of the 5-HT$_{2C}$R–PTEN interface provides a novel way to enhance the efficacy of 5-HT$_{2C}$R signaling. Thus, 3L4F and its derivatives should be useful allosteric 5-HT$_{2C}$R-interacting ligands for use *in vivo*.

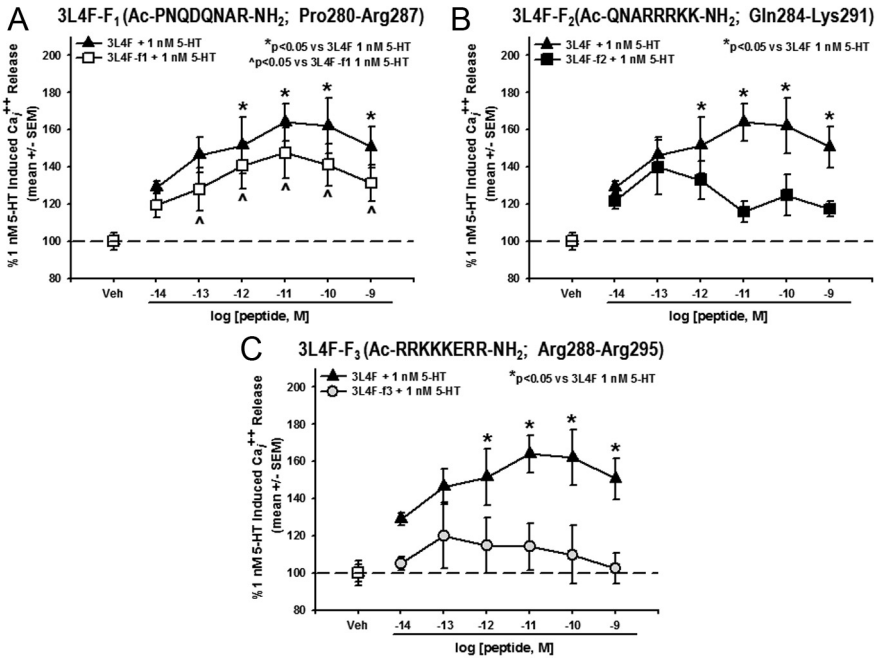

Figure 8. The active fragment of 3L4F is a component of its first 8 aa span. ***A***, Preincubation with human 3L4F-F$_1$ (15 min) dose dependently (10^{-13} to 10^{-9} M) increased Ca_i^{2+} release versus 1 nM 5-HT-evoked Ca_i^{2+} release in the 5-HT$_{2C}$R–CHO cells (*$p < 0.05$ vs 1 nM 5-HT; △) with similar efficacy as the lead peptide 3L4F (▲). ***B***, The human 3L4F-F$_2$ peptide did not alter Ca_i^{2+} release versus 1 nM 5-HT-evoked Ca_i^{2+} release in the 5-HT$_{2C}$R–CHO cells (■). ***C***, The human 3L4F-F$_3$ peptide did not alter Ca_i^{2+} release versus 1 nM 5-HT-evoked Ca_i^{2+} release in the 5-HT$_{2C}$R–CHO cells (□). Veh, Vehicle.

Mechanistic characterization of the efficacy of 3L4F as an adjuvant therapeutic in disorders characterized by 5-HT$_{2C}$R dysfunction within the limbic–corticostriatal circuit remains to be fully elucidated. Our data demonstrated that TAT conjugation is not necessary for cellular entry, although we have not determined whether enhanced transport across membranes will facilitate crossing of the blood–brain barrier. Nonetheless, the observation that systemic administration of a single, low dose of TAT–3L4F did not cause hypophagia, penile erection, or anxiogenesis but did suppress the development of a conditioned place preference to nicotine, as did a 5-HT$_{2C}$R agonist (Ji et al., 2006), suggests that this approach may prove therapeutically beneficial with a limited side-effect profile. Rat locomotor activity is an easily measurable dependent variable useful as a screen for pharmacological alterations of neuronal function, and 5-HT$_{2C}$R agonists are reported to dose dependently suppress both horizontal and vertical activity measures (Halford et al., 1997; Grottick et al., 2000; Fletcher et al., 2002; Halberstadt et al., 2009; Cunningham et al., 2011, 2012). Indeed, although a low dose of TAT–3L4F (0.1 μmol/kg) alone did not induce hypomotility (Ji et al., 2006; present study), this low dose augmented the effects of a selective 5-HT$_{2C}$R agonist to suppress locomotor activity. The TAT–3L4F peptide does possess 5-HT$_{2C}$R "agonist-like" properties at a higher dose (1 μmol/kg), exhibiting temporal- and dose-dependent suppression of spontaneous ambulation but not vertical activity. Thus, the 3L4F or peptide derivatives will be useful chemoprobes to dissect the role of the 5-HT$_{2C}$R–PTEN association in regulation of 5-HT$_{2C}$R function and to investigate the involvement of allosteric regulation over neurobiological processes.

Impulsivity has been defined clinically as a predisposition toward rapid unplanned reactions to stimuli without regard to the negative consequences (Moeller et al., 2001). Given the dynamic role of impulsivity in many chronic disorders involving 5-HT$_{2C}$R mechanisms and its place as a critical factor in treatment (Moeller et al., 2001), new medications that selectively enhance behavioral inhibition may facilitate recovery and abstinence. Clinical studies have consistently found an association between measures of 5-HT function and impulsivity (Virkkunen and Narvanen, 1987; Brown and Linnoila, 1990; Stein et al., 1993). With the accessibility to more selective pharmacologic tools, preclinical studies have gone one step further to identify pivotal and discriminating roles for 5-HT receptors, specifically 5-HT$_{2C}$R, in impulsivity (Pattij and Vanderschuren, 2008). Selective activation of 5-HT$_{2C}$R consistently reduces impulsivity, measured predominantly in 5-CSRT tasks (Winstanley et al., 2003; Fletcher et al., 2007; Navarra et al., 2008). Here, rats were treated with WAY163909 and evaluated in the 1-CSRT task (Anastasio et al., 2011; Cunningham et al., 2012), a variant of the 5-CSRT task (Dalley et al., 2002; Winstanley et al., 2004a), to determine the effects of a selective 5-HT$_{2C}$R agonist on impulsive action independent from complex visuospatial attention processes; the CSRT task tests the ability to withhold a prepotent response, similar to the continuous performance task used in humans (Robbins, 2002). In concordance with previous studies, WAY163909 potently suppressed impulsive action but did not alter additional measures of task performance, including accuracy, motiva-

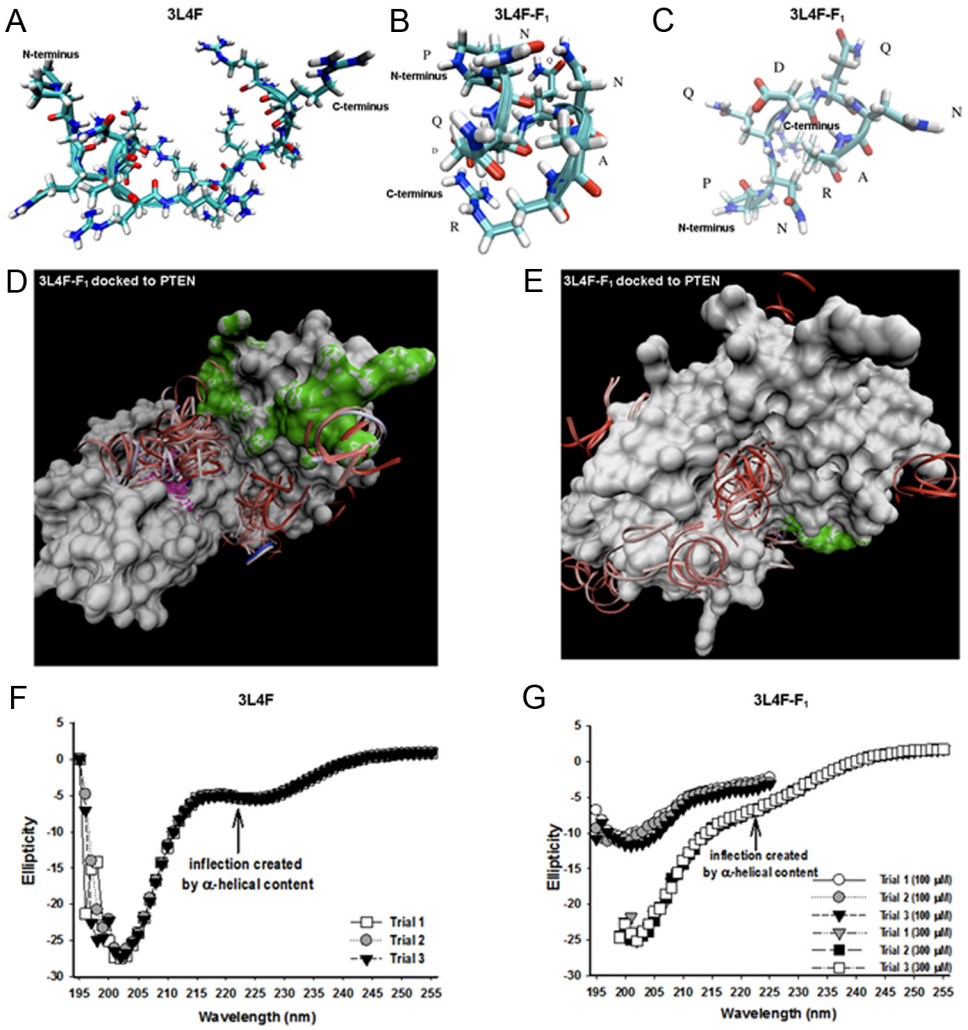

Figure 9. Molecular modeling of 3L4F and 3L4F-F$_1$ peptides against PTEN predict structural elements important for PTEN recognition and inhibition. ***A***, ***B***, The predicted conformation as derived from REMD simulations of the 3L4F peptide (***A***) displays α-helical content at the N terminus, which is conserved in the 3L4F-F$_1$ peptide (***B***) conformations. ***C***, The 3L4F-F1 peptide REMD simulations also predicted β-turn structure. ***D***, GRAMM dockings of the most populated α-helical conformation clustered in the central groove between the phosphatase active site and C2 membrane-targeting structural domains. The phosphatase active site of PTEN is denoted in purple, and the C2 membrane-targeting structural domain of PTEN is denoted in green. ***E***, GRAMM dockings of a less-populated cluster site of α-helical conformations was found on the immediately opposite side of the central groove. CD detects the presence of some α-helical content (inflection point at 222 nm) in the 3L4F (300 μM) (***F***) and 3L4F-F$_1$ peptide (100 and 300 μM) (***G***). Each peptide was subjected to three trial runs of CD.

tion, or motility indices. An effective allosteric disrupter of the 5-HT$_{2C}$R–PTEN interaction would be predicted to have limited behavioral effects alone but enhance the effects of low doses of a 5-HT$_{2C}$R agonist. In support of this hypothesis, the combination of ineffective doses of TAT–3L4F plus WAY163909 attenuated impulsive action indicative of an allosteric modulation of 5-HT$_{2C}$R function *in vivo*. Thus, the selective disruption of the 5-HT$_{2C}$R–PTEN association is a pharmacologic means to enhance 5-HT$_{2C}$R function with a potentially acceptable side-effect profile.

Biologically active peptides are important leads for medication and bioprobe development. The sequence of first starting with a peptide, then proceeding to pseudo-peptides (peptides with modified peptide bonds), followed by peptidomimetics, and finally to analogs (small molecules that differ significantly from the initial peptide) has been used to develop important therapeutic medications, such as angiotensin converting enzyme inhibitors (Meissner et al., 2002; Urbahns et al., 2003), Arg-Gly-Asp mimics (Greenspoon et al., 1993; Jones et al., 2003), and HIV protease inhibitors (Prabhakaran et al., 2002; Breccia et al., 2003). We have begun this process with synthesizing the lead peptide 3L4F and new peptide fragments of 3L4F to identify the active portion of the 3L4F peptide. In the present study, the 3L4F peptide was truncated into three overlapping 8 aa peptide fragments (3L4F-F$_1$, 3L4F-F$_2$, and 3L4F-F$_3$); derivative 3L4F-F$_1$ was the only derivative to maintain similar efficacy as the 3L4F peptide (within the picomolar range) to enhance 5-HT-evoked Ca_i^{2+} release in 5-HT$_{2C}$R–CHO cells, suggesting that these amino acid sites are the critical residues for activity of the 3L4F peptide. After the discovery of the minimum active peptide, molecular modeling was used to direct the future development of peptidomimetics that have greater stability and better activity than the small peptides. Toward that goal, 3L4F-F$_1$ peptide conformations were computationally predicted to populate both α-helix and β-turn secondary structures over the time course of the simulations. Moreover, coarse-grained docking of these peptide conformations against PTEN provide preliminary insight into potential interaction sites that clustered in the phosphatase active site and C2 membrane-targeting structural domain in-

terface of PTEN. Validation and refinement of the potential 3L4F-F_1 to the PTEN interaction site will be key in providing additional atomistic detail for pharmacophore model definition in the search for selective ligands active at that site.

The theoretical concept that the 5-HT_{2C}R–PTEN interface provides a novel target through which to modulate the output of the 5-HT_{2C}R signalosome is novel and supported by significant new evidence of the impact of this protein–protein interaction on 5-HT_{2C}R function. The results presented herein confirm the importance of the protein complex formation between the 5-HT_{2C}R and PTEN proteins in both heterologous and native tissues and indicate that disruption of the 5-HT_{2C}R–PTEN complex may be a viable approach to maintain and/or enhance the efficiency of 5-HT_{2C}R signaling. The ability to selectively target this protein–protein interaction for a receptor that is found predominately in the brain (Anastasio et al., 2010) also suggests that resultant therapeutic compounds will have very limited side-effect profiles. These data and the overall concept challenges and shifts the current paradigm of seeking new 5-HT_{2C}R medications through the development of ligands that act at the orthosteric binding site to new loci of interfaces between the 5-HT_{2C}R and other intracellular proteins. Such allosteric modulation of 5-HT_{2C}R signaling presents a new therapeutic approach in psychiatric disorders in which disrupted 5-HT_{2C}R signaling is implicated.

References

Aarts M, Liu Y, Liu L, Besshoh S, Arundine M, Gurd JW, Wang YT, Salter MW, Tymianski M (2002) Treatment of ischemic brain damage by perturbing NMDA receptor- PSD-95 protein interactions. Science 298:846–850. CrossRef Medline

Abbas AI, Yadav PN, Yao WD, Arbuckle MI, Grant SG, Caron MG, Roth BL (2009) PSD-95 is essential for hallucinogen and atypical antipsychotic drug actions at serotonin receptors. J Neurosci 29:7124–7136. CrossRef Medline

Agnati LF, Guidolin D, Leo G, Guescini M, Pizzi M, Stocchi V, Spano PF, Ghidoni R, Ciruela F, Genedani S, Fuxe K (2011) Possible new targets for GPCR modulation: allosteric interactions, plasma membrane domains, intercellular transfer and epigenetic mechanisms. J Recept Signal Transduct Res 31:315–331. CrossRef Medline

Anastasio NC, Lanfranco MF, Bubar MJ, Seitz PK, Stutz SJ, McGinnis AG, Watson CS, Cunningham KA (2010) Serotonin 5-HT2C receptor protein expression is enriched in synaptosomal and post-synaptic compartments of rat cortex. J Neurochem 113:1504–1515. CrossRef Medline

Anastasio NC, Stoffel EC, Fox RG, Bubar MJ, Rice KC, Moeller FG, Cunningham KA (2011) Serotonin (5-hydroxytryptamine) 5-HT_{2A} receptor: association with inherent and cocaine-evoked behavioral disinhibition in rats. Behav Pharmacol 22:248–261. CrossRef Medline

Backstrom JR, Price RD, Reasoner DT, Sanders-Bush E (2000) Deletion of the serotonin 5-HT2C receptor PDZ recognition motif prevents receptor phosphorylation and delays resensitization of receptor responses. J Biol Chem 275:23620–23626. CrossRef Medline

Bécamel C, Alonso G, Galéotti N, Demey E, Jouin P, Ullmer C, Dumuis A, Bockaert J, Marin P (2002) Synaptic multiprotein complexes associated with 5-HT(2C) receptors: a proteomic approach. EMBO J 21:2332–2342. CrossRef Medline

Bechara A, Dolan S, Denburg N, Hindes A, Anderson SW, Nathan PE (2001) Decision-making deficits, linked to a dysfunctional ventromedial prefrontal cortex, revealed in alcohol and stimulant abusers. Neuropsychologia 39:376–389. CrossRef Medline

Berg KA, Clarke WP, Sailstad C, Saltzman A, Maayani S (1994) Signal transduction differences between 5-hydroxytryptamine type 2A and type 2C receptor systems. Mol Pharmacol 46:477–484. Medline

Berg KA, Maayani S, Goldfarb J, Scaramellini C, Leff P, Clarke WP (1998) Effector pathway-dependent relative efficacy at serotonin type 2A and 2C receptors: evidence for agonist-directed trafficking of receptor stimulus. Mol Pharmacol 54:94–104. Medline

Berg KA, Stout BD, Maayani S, Clarke WP (2001) Differences in rapid desensitization of 5-hydroxytryptamine2A and 5-hydroxytryptamine2C receptor-mediated phospholipase C activation. J Pharmacol Exp Ther 299:593–602. Medline

Breccia P, Boggetto N, Pérez-Fernández R, Van Gool M, Takahashi M, Ren é L, Prados P, Badet B, Reboud-Ravaux M, de Mendoza J (2003) Dimerization inhibitors of HIV-1 protease based on a bicyclic guanidinium subunit. J Med Chem 46:5196–5207. CrossRef Medline

Brown GL, Linnoila MI (1990) CSF serotonin metabolite (5-HIAA) studies in depression, impulsivity, and violence. J Clin Psychiatry [Suppl] 51:31–41. Medline

Bubar MJ, Cunningham KA (2008) Prospects for serotonin 5-HT_2R pharmacotherapy in psychostimulant abuse. Prog Brain Res 172:319–346. CrossRef Medline

Chen YH, Yang JT, Chau KH (1974) Determination of the helix and beta form of proteins in aqueous solution by circular dichroism. Biochemistry 13:3350–3359. CrossRef Medline

Cheung AH, Huang RR, Strader CD (1992) Involvement of specific hydrophobic, but not hydrophilic, amino acids in the third intracellular loop of the beta-adrenergic receptor in the activation of Gs. Mol Pharmacol 41:1061–1065. Medline

Conn PJ, Christopoulos A, Lindsley CW (2009) Allosteric modulators of GPCRs: a novel approach for the treatment of CNS disorders. Nat Rev Drug Discov 8:41–54. CrossRef Medline

Cunningham KA, Fox RG, Anastasio NC, Bubar MJ, Stutz SJ, Moeller FG, Gilbertson SR, Rosenzweig-Lipson S (2011) Selective serotonin 5-HT2C receptor activation suppresses the reinforcing efficacy of cocaine and sucrose but differentially affects the incentive-salience value of cocaine- vs. sucrose-associated cues. Neuropharmacology 61:513–523. CrossRef Medline

Cunningham KA, Anastasio NC, Fox RG, Stutz SJ, Bubar MJ, Swinford SE, Watson CS, Gilbertson SR, Rice KC, Rosenzweig-Lipson S, Moeller FG (2012) Synergism between a serotonin 5-HT_{2A} receptor (5-HT_{2A}R) antagonist and 5-HT_{2C}R agonist suggests new pharmacotherapeutics for cocaine addiction. ACS Chem Neurosci. Advance online publication. Retrieved December 11, 2012. doi:10.1021/cn300072u. CrossRef

Dalley JW, Theobald DE, Eagle DM, Passetti F, Robbins TW (2002) Deficits in impulse control associated with tonically-elevated serotonergic function in rat prefrontal cortex. Neuropsychopharmacology 26:716–728. CrossRef Medline

Ding C, Bremer NM, Smith TD, Seitz PK, Anastasio NC, Cunningham KA, Zhou J (2012) Exploration of synthetic approaches and pharmacological evaluation of PNU-69176E and its stereoisomer as 5-HT_{2C} receptor allosteric modulators. ACS Chem Neurosci 3:538–545. CrossRef Medline

Dunlop J, Marquis KL, Lim HK, Leung L, Kao J, Cheesman C, Rosenzweig-Lipson S (2006) Pharmacological profile of the 5-HT(2C) receptor agonist WAY-163909; therapeutic potential in multiple indications. CNS Drug Rev 12:167–177. CrossRef Medline

Fletcher PJ, Grottick AJ, Higgins GA (2002) Differential effects of the 5-HT2A receptor antagonist M100,907 and the 5-HT2C receptor antagonist SB242,084 on cocaine-induced locomotor activity, cocaine self-administration and cocaine-induced reinstatement of responding. Neuropsychopharmacology 27:576–586. CrossRef Medline

Fletcher PJ, Tampakeras M, Sinyard J, Higgins GA (2007) Opposing effects of 5-HT(2A) and 5-HT(2C) receptor antagonists in the rat and mouse on premature responding in the five-choice serial reaction time test. Psychopharmacology (Berl) 195:223–234. CrossRef Medline

Gavarini S, Bécamel C, Altier C, Lory P, Poncet J, Wijnholds J, Bockaert J, Marin P (2006) Opposite effects of PSD-95 and MPP3 PDZ proteins on serotonin 5-hydroxytryptamine2C receptor desensitization and membrane stability. Mol Biol Cell 17:4619–4631. CrossRef Medline

Glykos NM (2006) Software news and updates. Carma: a molecular dynamics analysis program. J Comput Chem 27:1765–1768. CrossRef Medline

Goldstein RZ, Tomasi D, Rajaram S, Cottone LA, Zhang L, Maloney T, Telang F, Alia-Klein N, Volkow ND (2007) Role of the anterior cingulate and medial orbitofrontal cortex in processing drug cues in cocaine addiction. Neuroscience 144:1153–1159. CrossRef Medline

Greenfield N, Fasman GD (1969) Computed circular dichroism spectra for the evaluation of protein conformation. Biochemistry 8:4108–4116. CrossRef Medline

Greenspoon N, Hershkoviz R, Alon R, Varon D, Shenkman B, Marx G, Federman S, Kapustina G, Lider O (1993) Structural analysis of integrin recognition and the inhibition of integrin-mediated cell functions by

novel nonpeptidic surrogates of the Arg-Gly-Asp sequence. Biochemistry 32:1001–1008. CrossRef Medline

Grottick AJ, Fletcher PJ, Higgins GA (2000) Studies to investigate the role of 5-HT(2C) receptors on cocaine- and food-maintained behavior. J Pharmacol Exp Ther 295:1183–1191. Medline

Halberstadt AL, van der Heijden I, Ruderman MA, Risbrough VB, Gingrich JA, Geyer MA, Powell SB (2009) 5-HT(2A) and 5-HT(2C) receptors exert opposing effects on locomotor activity in mice. Neuropsychopharmacology 34:1958–1967. CrossRef Medline

Halford JC, Lawton CL, Blundell JE (1997) The 5-HT2 receptor agonist MK-212 reduces food intake and increases resting but prevents the behavioural satiety sequence. Pharmacol Biochem Behav 56:41–46. CrossRef Medline

Heffner TG, Hartman JA, Seiden LS (1980) Rapid method for the regional dissection of the rat brain. Pharmacol Biochem Behav 13:453–456. CrossRef Medline

Heisler LK, Cowley MA, Kishi T, Tecott LH, Fan W, Low MJ, Smart JL, Rubinstein M, Tatro J, Zigman JM, Cone RD, Elmquist JK (2003) Central serotonin and melanocortin pathways regulating energy homeostasis. Ann N Y Acad Sci 994:169–174. CrossRef Medline

Holde K, Johnson WC, Ho PS (1998) Principles of physical biochemistry. Englewood Cliffs, NJ: Prentice-Hall.

Im WB, Chio CL, Alberts GL, Dinh DM (2003) Positive allosteric modulator of the human 5-HT2C receptor. Mol Pharmacol 64:78–84. CrossRef Medline

Ji SP, Zhang Y, Van Cleemput J, Jiang W, Liao M, Li L, Wan Q, Backstrom JR, Zhang X (2006) Disruption of PTEN coupling with 5-HT2C receptors suppresses behavioral responses induced by drugs of abuse. Nat Med 12:324–329. CrossRef Medline

Jones RM, Boatman PD, Semple G, Shin YJ, Tamura SY (2003) Clinically validated peptides as templates for de novo peptidomimetic drug design at G-protein-coupled receptors. Curr Opin Pharmacol 3:530–543. CrossRef Medline

Julius D, MacDermott AB, Axel R, Jessell TM (1988) Molecular characterization of a functional cDNA encoding the serotonin 1C receptor. Science 241:558–564. CrossRef Medline

Julius D, Livelli TJ, Jessell TM, Axel R (1989) Ectopic expression of the serotonin 1C receptor and the triggering of malignant transformation. Science 244:1057–1062. CrossRef Medline

Kenakin T (2010) G protein coupled receptors as allosteric proteins and the role of allosteric modulators. J Recept Signal Transduct Res 30: 313–321. CrossRef Medline

Kennett GA, Clifton PG (2010) New approaches to the pharmacological treatment of obesity: can they break through the efficacy barrier? Pharmacol Biochem Behav 97:63–83. CrossRef Medline

Keov P, Sexton PM, Christopoulos A (2011) Allosteric modulation of G protein-coupled receptors: a pharmacological perspective. Neuropharmacology 60:24–35. CrossRef Medline

Keppel G (1973) Design and analysis: a researcher's handbook. Englewood Cliffs, NJ: Prentice-Hall.

Labasque M, Reiter E, Becamel C, Bockaert J, Marin P (2008) Physical interaction of calmodulin with the 5-hydroxytryptamine2C receptor C-terminus is essential for G protein-independent, arrestin-dependent receptor signaling. Mol Biol Cell 19:4640–4650. CrossRef Medline

Li X, Latour RA, Stuart SJ (2009) TIGER2: an improved algorithm for temperature intervals with global exchange of replicas. J Chem Phys 130: 174106. CrossRef Medline

Liu S, Bubar MJ, Lanfranco MF, Hillman GR, Cunningham KA (2007) Serotonin(2C) receptor localization in GABA neurons of the rat medial prefrontal cortex: implications for understanding the neurobiology of addiction. Neuroscience 146:1667–1688. CrossRef Medline

MacKerell AD, Bashford D, Bellot M, Dunbrack RL, Evanseck JD, Field MJ, Fischer S, Gao J, Guo H, Ha S, Jospeh-McCarthy D, Kuchnir L, Kuczera K, Lau FT, Mattos C, Michnick S, Ngo T, Nguyen DT, Prodhom B, Reiher WE, et al. (1998) All-atom empirical potential for molecular modeling and dynamics: studies of proteins. J Phys Chem B 102:3586–3616. CrossRef

Meissner RS, Perkins JJ, Duong le T, Hartman GD, Hoffman WF, Huff JR, Ihle NC, Leu CT, Nagy RM, Naylor-Olsen A, Rodan GA, Rodan SB, Whitman DB, Wesolowski GA, Duggan ME (2002) Nonpeptide alpha(v)beta(3) antagonists. Part 2: constrained glycyl amides derived from the RGD tripeptide. Bioorg Med Chem Lett 12:25–29. CrossRef Medline

Melancon BJ, Hopkins CR, Wood MR, Emmitte KA, Niswender CM, Christopoulos A, Conn PJ, Lindsley CW (2012) Allosteric modulation of seven transmembrane spanning receptors: theory, practice, and opportunities for central nervous system drug discovery. J Med Chem 55:1445–1464. CrossRef Medline

Mengod G, Pompeiano M, Martínez-Mir MI, Palacios JM (1990) Localization of the mRNA for the 5-HT_2 receptor by in situ hybridization histochemistry. Correlation with the distribution of receptor sites. Brain Res 524:139–143. CrossRef Medline

Mengod G, Vilar ó MT, Raurich A, López-Giménez JF, Cortés R, Palacios JM (1996) 5-HT receptors in mammalian brain: receptor autoradiography and in situ hybridization studies of new ligands and newly identified receptors. Histochem J 28:747–758. CrossRef Medline

Millan MJ, Marin P, Bockaert J, Mannoury la Cour C (2008) Signaling at G-protein-coupled serotonin receptors: recent advances and future research directions. Trends Pharmacol Sci 29:454–464. CrossRef Medline

Moeller FG, Dougherty DM, Barratt ES, Schmitz JM, Swann AC, Grabowski J (2001) The impact of impulsivity on cocaine use and retention in treatment. J Subst Abuse Treat 21:193–198. CrossRef Medline

Moya PR, Berg KA, Gutiérrez-Hernandez MA, Sáez-Briones P, Reyes-Parada M, Cassels BK, Clarke WP (2007) Functional selectivity of hallucinogenic phenethylamine and phenylisopropylamine derivatives at human 5-hydroxytryptamine (5-HT)2A and 5-HT2C receptors. J Pharmacol Exp Ther 321:1054–1061. CrossRef Medline

Müller D, Mukhopadhyay AK, Davidoff MS, Middendorff R (2011) Cyclic GMP signaling in rat urinary bladder, prostate, and epididymis: tissue-specific changes with aging and in response to Leydig cell depletion. Reproduction 142:333–343. CrossRef Medline

Navarra R, Comery TA, Graf R, Rosenzweig-Lipson S, Day M (2008) The 5-HT(2C) receptor agonist WAY-163909 decreases impulsivity in the 5-choice serial reaction time test. Behav Brain Res 188:412–415. CrossRef Medline

Pattij T, Vanderschuren LJ (2008) The neuropharmacology of impulsive behaviour. Trends Pharmacol Sci 29:192–199. CrossRef Medline

Phillips JC, Braun R, Wang W, Gumbart J, Tajkhorshid E, Villa E, Chipot C, Skeel RD, Kal é L, Schulten K (2005) Scalable molecular dynamics with NAMD. J Comput Chem 26:1781–1802. CrossRef Medline

Pompeiano M, Palacios JM, Mengod G (1994) Distribution of the serotonin 5-HT_2 receptor family mRNAs: comparison between 5-HT_{2A} and 5-HT_{2C} receptors. Mol Brain Res 23:163–178. CrossRef Medline

Prabhakaran EN, Rao IN, Boruah A, Iqbal J (2002) Synthesis of small cyclic peptides via reverse turn induced ring closing metathesis of tripeptides. J Org Chem 67:8247–8250. CrossRef Medline

Price DJ, Brooks CL 3rd (2004) A modified TIP3P water potential for simulation with Ewald summation. J Chem Phys 121:10096–10103. CrossRef Medline

Raymond JR, Mukhin YV, Gelasco A, Turner J, Collinsworth G, Gettys TW, Grewal JS, Garnovskaya MN (2001) Multiplicity of mechanisms of serotonin receptor signal transduction. Pharmacol Ther 92:179–212. CrossRef Medline

Robbins TW (2002) The 5-choice serial reaction time task: behavioural pharmacology and functional neurochemistry. Psychopharmacology (Berl) 163:362–380. CrossRef Medline

Rosenzweig-Lipson S (2011) New horizons for selective 5-HT2C receptor ligands in psychiatric/neurological disorders. Neuropsychopharmacology 36:363–364. CrossRef Medline

Rosenzweig-Lipson S, Zhang J, Mazandarani H, Harrison BL, Sabb A, Sabalski J, Stack G, Welmaker G, Barrett JE, Dunlop J (2006) Antiobesity-like effects of the 5-HT(2C) receptor agonist WAY-161503. Brain Res 1073–1074:240–251. CrossRef

Schwarze SR, Ho A, Vocero-Akbani A, Dowdy SF (1999) In vivo protein transduction: delivery of a biologically active protein into the mouse. Science 285:1569–1572. CrossRef Medline

Seitz PK, Bremer NM, McGinnis AG, Cunningham KA, Watson CS (2012) Quantitative changes in intracellular calcium and extracellular-regulated kinase activition in CHO cells stably expressing serotonin (5-HT) 5-HT_{2A} or 5-HT_{2C} receptors. BMC Neuroscience 13:25. CrossRef Medline

Shashack MJ, Cunningham KA, Seitz PK, McGinnis A, Smith T, Watson CS, Gilbertson SR (2011) Synthesis and evaluation of dimeric derivatives of 5-HT(2A) receptor (5-HT(2A)R) antagonist M-100907. ACS Chem Neurosci 2:640–644. CrossRef Medline

Söderberg O, Gullberg M, Jarvius M, Ridderstråle K, Leuchowius KJ, Jarvius

J, Wester K, Hydbring P, Bahram F, Larsson LG, Landegren U (2006) Direct observation of individual endogenous protein complexes in situ by proximity ligation. Nat Methods 3:995–1000. CrossRef Medline

Stein DJ, Hollander E, Liebowitz MR (1993) Neurobiology of impulsivity and the impulse control disorders. J Neuropsychiatry 5:9–17. Medline

Stout BD, Clarke WP, Berg KA (2002) Rapid desensitization of the serotonin(2C) receptor system: effector pathway and agonist dependence. J Pharmacol Exp Ther 302:957–962. CrossRef Medline

Sugita Y, Okamoto Y (1999) Replica-exchange molecular dynamics method for protein folding. Chem Phys Letters 314:261. CrossRef

Tesmer JJ (2006) Pharmacology. Hitting the hot spots of cell signaling cascades. Science 312:377–378. CrossRef Medline

Trifilieff P, Rives ML, Urizar E, Piskorowski RA, Vishwasrao HD, Castrillon J, Schmauss C, Slättman M, Gullberg M, Javitch JA (2011) Detection of antigen interactions ex vivo by proximity ligation assay: endogenous dopamine D2-adenosine A2A receptor complexes in the striatum. BioTechniques 51:111–118. Medline

Urbahns K, Härter M, Vaupel A, Albers M, Schmidt D, Brüggemeier U, Stelte-Ludwig B, Gerdes C, Tsujishita H (2003) Biphenyls as potent vitronectin receptor antagonists. Part 2: biphenylalanine ureas. Bioorg Med Chem Lett 13:1071–1074. CrossRef Medline

Vakser IA, Aflalo C (1994) Hydrophobic docking: a proposed enhancement to molecular recognition techniques. Proteins 20:320–329. CrossRef Medline

Virkkunen M, Närvänen S (1987) Plasma insulin, tryptophan and serotonin levels during the glucose tolerance test among habitually violent and impulsive offenders. Neuropsychobiology 17:19–23. CrossRef Medline

Watson CS, Jeng YJ, Hu G, Wozniak A, Bulayeva N, Guptarak J (2012) Estrogen- and xenoestrogen-induced ERK signaling in pituitary tumor cells involves estrogen receptor-alpha interactions with G protein-alphai and caveolin I. Steroids 77:424–432. CrossRef Medline

Winstanley CA, Chudasama Y, Dalley JW, Theobald DE, Glennon JC, Robbins TW (2003) Intra-prefrontal 8-OH-DPAT and M100907 improve visuospatial attention and decrease impulsivity on the five-choice serial reaction time task in rats. Psychopharmacology (Berl) 167:304–314. Medline

Winstanley CA, Dalley JW, Theobald DE, Robbins TW (2004a) Fractionating impulsivity: contrasting effects of central 5-HT depletion on different measures of impulsive behavior. Neuropsychopharmacology 29:1331–1343. CrossRef Medline

Winstanley CA, Theobald DE, Dalley JW, Glennon JC, Robbins TW (2004b) 5-HT2A and 5-HT2C receptor antagonists have opposing effects on a measure of impulsivity: interactions with global 5-HT depletion. Psychopharmacology (Berl) 176:376–385. CrossRef Medline